Title

Influence of Nanomolar Deltamethrin on the Hallmarks of Primary Cultured Cortical Neuronal Network and the Role of Ryanodine Receptors.

Journal

Environmental health perspectives, 127(6)

ISSN

0091-6765

Authors

Zheng, Jing
Yu, Yiyi
Feng, Wei
et al.

Publication Date

2019-06-01

DOI

10.1289/ehp4583

Peer reviewed

A Section 508–conformant HTML version of this article is available at https://doi.org/10.1289/EHP4583.

Influence of Nanomolar Deltamethrin on the Hallmarks of Primary Cultured Cortical Neuronal Network and the Role of Ryanodine Receptors

Jing Zheng,[1,2] Yiyi Yu,[1]* Wei Feng,[2] Jing Li,[1] Ju Liu,[1] Chunlei Zhang,[1] Yao Dong,[2] Isaac N. Pessah,[2] and Zhengyu Cao[1]*

[1]State Key Laboratory of Natural Medicines, Jiangsu Provincial Key Laboratory for TCM Evaluation and Translational Research, Department of TCM Pharmacology, School of Traditional Pharmacy, China Pharmaceutical University, Nanjing, China
[2]Department of Molecular Biosciences, School of Veterinary Medicine, University of California, Davis, California, USA

Background: The pyrethroid deltamethrin (DM) is broadly used for insect control. Although DM hyperexcites neuronal networks by delaying inactivation of axonal voltage-dependent Na^+ channels, this mechanism is unlikely to mediate neurotoxicity at lower exposure levels during critical perinatal periods in mammals.

Objectives: We aimed to identify mechanisms by which acute and subchronic DM altered axonal and dendritic growth, patterns of synchronous Ca^{2+} oscillations (SCOs), and electrical spike activity (ESA) functions critical to neuronal network formation.

Methods: Measurements of SCOs using Ca^{2+} imaging, ESA using microelectrode array (MEA) technology, and dendritic complexity using Sholl analysis were performed in primary murine cortical neurons from wild-type (WT) and/or ryanodine receptor 1 ($RyR1^{T4826I/T4826I}$) mice between 5 and 14 d *in vitro* (DIV). [^{3}H]ryanodine binding analysis and a single-channel voltage clamp were utilized to measure engagement of RyRs as a direct target of DM.

Results: Neuronal networks responded to DM (30–70 nM) as early as 5 DIV, reducing SCO amplitude and depressing ESA and burst frequencies by 60–70%. DM (10–300 nM) enhanced axonal growth in a nonmonotonic manner. DM ≥100 nM enhanced dendritic complexity. DM stabilized channel open states of RyR1, RyR2, and cortical preparations expressing all three isoforms. DM (30 nM) altered gating kinetics of RyR1 channels, increasing mean open time, decreasing mean closed time, and thereby enhancing overall open probability. SCO patterns from cortical networks expressing $RyR1^{T4826I/T4826I}$ were more responsive to DM than WT. $RyR1^{T4826I/T4826I}$ neurons showed inherently longer axonal lengths than WT neurons and maintained less length-promoting responses to nanomolar DM.

Conclusions: Our findings suggested that RyRs were sensitive molecular targets of DM with functional consequences likely relevant for mediating abnormal neuronal network connectivity *in vitro*. https://doi.org/10.1289/EHP4583

Introduction

Pyrethroids are synthetic insecticides that structurally mimic pyrethrins derived from the flower of *Chrysanthemum* sp. (Casida and Quistad 1998). Pyrethroids account for approximately 25% of the insecticidal market worldwide with increasing usage due to the ban of organophosphates for home use in many countries, including the United States (Amweg et al. 2005; Gan 2008). The extensive use of pyrethroids for domestic, industrial, and agricultural settings increases the potential of exposure through multiple routes, especially to susceptible populations, including children and pregnant women (Saillenfait et al. 2015). Pyrethroids are heuristically divided into two major groups according to their structural properties and acute intoxication syndromes. Type I pyrethroids lacking a cyano moiety at the α carbon of the 3-phenoxybenzyl alcohol moiety produce tremor syndrome, including hyperexcitation, tremors, and convulsions, whereas Type II pyrethroids possessing an α–cyano group induce choreoathetosis and salivation syndrome, characterized as hypersensitivity, choreoathetosis, salivation, and seizures (Soderlund et al. 2002; Wolansky and Harrill 2008). A few pyrethroids produce mixed signs, including both tremors and salivation, and are classified as Type I/II (Soderlund et al. 2002; Wolansky and Harrill 2008).

Pyrethroids have been demonstrated to interact with several types of ion channels, including voltage-gated calcium channels (Li et al. 2018; Meijer et al. 2014), two-pore domain potassium channels (Castellanos et al. 2018), and voltage-dependent chloride channels (Forshaw et al. 1993; Taylor-Wells et al. 2015). Historically, the acute neurotoxicity of pyrethroids have been attributed to their ability to selectively bind to axonal voltage-gated sodium channels (VGSCs) (Cao et al. 2011a; Clark and Symington 2012; Soderlund 2012). Pyrethroids delay inactivation kinetics of VGSCs, resulting in altered patterns of neuronal excitability manifested both *in vitro* and *in vivo* by increased neuronal firing rates with epochs of repetitive discharges or depolarizing block of neurotransmission (Clark and Symington 2012; Narahashi 1985; Soderlund 2012; Vijverberg et al. 1982). However, a consistent observation across studies indicates that concentrations >10 μM are necessary to elicit changes in mammalian VGSC function for many pyrethroids (Clark and Symington 2012; Field et al. 2017).

Pyrethroids or the major pyrethroid metabolites, 3-phenoxybenzoic acid (3-PBA), *cis*-3-(2,2-dichlorovinyl)-2,2-dimethyl-(1-cyclopropane) carboxylic acid (*cis*-DCCA), and *trans*-3-(2,2-dichlorovinyl)-2,2-dimethyl-(1-cyclopropane) carboxylic acid (*trans*-DCCA) have been detected in most environmental samples collected from homes (Morgan et al. 2007; Qi et al. 2012; Wu et al. 2013) and child care facilities (Morgan et al. 2007), as well as urinary samples collected from mothers (Dereumeaux et al. 2018; Qi et al. 2012) and children (Dereumeaux et al. 2018; Qi et al. 2012; Wu et al. 2013). Exposures varied with geographic location as listed in Table 1 and were correlated to patterns of pyrethroid use (Morgan et al. 2007; Oulhote and Bouchard 2013; Wu et al. 2013). The total level of three pyrethroid metabolites could reach as high

*These authors contributed equally to this work.
Address correspondence to Zhengyu Cao, Ph.D., Department of TCM Pharmacology, School of Traditional Chinese Pharmacy, China Pharmaceutical University, 639 Longmian Ave., Jiangning District, Nanjing 211198, China. Email: zycao1999@hotmail.com; and Isaac N. Pessah, Ph.D., Department of Molecular Biosciences, School of Veterinary Medicine, University of California, Davis, 1020 VM3B 1089 Veterinary Medicine Way, Davis, CA 95616-5270, USA. Email: Inpessah@ucdavis.edu

Supplemental Material is available online (https://doi.org/10.1289/EHP4583).
The authors declare that they have no actual or potential competing financial interests.
Received 11 October 2018; Revised 9 May 2019; Accepted 10 May 2019; Published 5 June 2019.

Table 1. Concentrations of urinary pyrethroid metabolites in different populations.

Metabolites by sample source	Exposure levels (μg/L)		References
	Median concentration	Maximal concentration	
Children at 6–11 y of age (Canada)	—	—	(Oulhote and Bouchard 2013)
3-PBA	0.2	32	—
cis-DBCA	<0.006	2	—
cis-DCCA	0.05	6	—
trans-DCCA	0.15	41	—
Infants at 12 months of age (China)	—	—	(Wu et al. 2013)
3-PBA	0.39	90.26	—
cis-DCCA	0.18	6.82	—
trans-DCCA	0.92	236.28	—
Pregnant women (China)	—	—	(Xue et al. 2013)
3-PBA	2.24	52.13	—
cis-DCCA	1.22	80.19	—
trans-DCCA	3.65	85.26	—
Preschool children (Ohio, United States)	—	—	(Morgan et al. 2007)
3-PBA	0.3	33.3	—

Note: —, no data; *cis*-DBCA, *cis*-(2,2-dibromovinyl)-2,2-dimethylcyclopropane-1-carboxylic acid; *cis*-DCCA, *cis*-(2,2-dichlorovinyl)-2,2-dimethylcyclopropane-1-carboxylic acid; *trans*-DCCA, *trans*-(2,2-dichlorovinyl)-2,2-dimethylcyclopropane-1-carboxylic acid; 3-PBA, 3-phenoxybenzoic acid.

as 262 ng/mL (Wu et al. 2013). In addition to the urinary samples, human breast milk also contained pyrethroids whose levels varied widely (Corcellas et al. 2012; Sharma et al. 2014), a consequence likely resulting from differential exposures. Thus, pyrethroid exposure during the perinatal and early childhood periods may contribute to increased risks for neurotoxicity. Results from two recent studies based on residential proximity to agricultural pesticides in California suggested an association between prenatal exposure to pyrethroids and increased risks for attention-deficit/hyperactivity disorder (ADHD) (Shelton et al. 2014) and delayed perceptual reasoning and verbal comprehension scores (Gunier et al. 2017). Results from a study of pyrethroid exposure during pregnancy in China identified associations between pyrethroid metabolites in maternal urine with adverse outcomes on the growth and development of infants (Xue et al. 2013). Although a high concentration of 3-PBA has been detected in urinary samples, 3-PBA did not affect the viability of SH-SY5Y cells at concentrations as high as 100 μM (Romero et al. 2012).

Mice exposed prenatally to low doses (0.3 mg/kg and 1 mg/kg) of deltamethrin (DM), a Type II pyrethroid, displayed ADHD-like behavior including hyperactivity, working memory and attention deficits, and impulsive-like behaviors that were presumably mediated by altered dopaminergic signal pathways (Richardson et al. 2015). The concentration of DM in brain tissue has been shown to reach ∼16 ng/g (30 nM) after a single oral dose of 0.5 mg/kg DM in postnatal day 21 rats (Mortuza et al. 2018).

Primary cortical neurons exhibit spontaneous electrical discharges consisting of infrequent synchronized as well as desynchronized randomized field potentials as they formed functional neuronal networks (Cao et al. 2014b; Frega et al. 2012). Developing neuronal networks also display spontaneous synchronized Ca^{2+} oscillations (SCOs) (Cao et al. 2012a), whose patterns depend on the balance of excitatory and inhibitory neurotransmission within the neuronal network (Pacico and Mingorance-Le Meur 2014). SCOs are orchestrated by multiple Ca^{2+} signaling pathways that are highly integrated and regulated (Dravid and Murray 2004). SCOs depend on electrical spike activity (ESA) (Spitzer et al. 1995), and both are crucial for neuronal development, activity-dependent neurite outgrowth, and network plasticity (Dolmetsch et al. 1998; Spitzer et al. 1995; Wayman et al. 2006). During early development *in vitro*, dendritic arborization, axonal elongation, and synapse formation form extensive neuronal network at around 6 d *in vitro* (DIV) (George et al. 2012; Harrill et al. 2011). Consistent with morphological development, electric spiking activity occurs as early as 3 DIV (Siebler et al. 1993), whereas the synchrony of spike activity (Cotterill et al. 2016; Frega et al. 2012) as well as SCOs (Cao et al. 2015; Cao et al. 2017) manifest after 6 DIV and gradually increase and stabilize between 10–12 DIV, at which time they exhibit long-distance network connectivity. We previously demonstrated that at relatively high concentrations (>1 μM), DM triggered a long-lived elevation of cytosolic intracellular Ca^{2+} concentrations primarily mediated by enhanced influx of extracellular Ca^{2+} that occurred concomitantly with depolarization of the neuronal (Cao et al. 2011b). This Ca^{2+} influx in primary cortical neurons cultured from rat was closely associated with changes in the expression of brain-derived neurotrophic factor (*Bdnf*) (Ihara et al. 2011, 2012). However, a lower concentration of DM (0.3 μM) decreased the SCO amplitude without detectable changes in the baseline intracellular Ca^{2+} concentration (Cao et al. 2011b). Ryanodine receptors (RyRs), together with inositol-1,4,5-trisphosphate receptors (IP_3R) influence Ca^{2+} release from sarcoplasmic reticulum/endoplasmic reticulum (SR/ER) stores, and thus mediate a myriad of Ca^{2+}-regulated cellular processes (Lanner et al. 2010; Pessah et al. 2010). Initial screening showed that DM at 5 μM increased [^{3}H]ryanodine ([^{3}H]Ry) binding to membrane vesicles, suggesting its direct activation of RyRs (Morisseau et al. 2009), an intracellular Ca^{2+} channel localized to the endoplasmic reticulum crucial for regulating Ca^{2+} dynamics and activity-dependent dendritic growth (Wayman et al. 2012a, 2012b). Although it has become clear that DM may alter Ca^{2+} dynamics in neurons, more information is needed to understand the impact on hallmarks of neuronal morphology and electric activity at concentrations more relevant to current human tissue levels (nanomolar concentration) and to clarify the potential mechanisms, especially those targeting RyRs.

We posited that environmental relevant level of DM could alter the morphological complexity and patterns of network activity within primary cultured cortical neurons that were mediated by altered activities of RyR channels within the same concentration range. Here we provide, to our knowledge, the first detailed investigation of how nanomolar DM influenced Ca^{2+} dynamics, ESA, and morphological complexity in cortical neurons cultured from wild-type (WT) and $RyR1^{T4826I/T4826I}$ mice. Considering their implication in neurotoxicity, we directly investigated how nanomolar DM influenced gating kinetics of RyRs. Our new findings are likely relevant for understanding the biological plausibility and molecular mechanisms mediating abnormal neuronal network formation and function-associated DM exposures.

Materials and Methods

Animals and Reagents

Male and female WT C57BL/6J mice purchased from the Jackson Laboratory and RyR1$^{T4826I/T4826I}$ knock-in C57BL/6J mice established as previous described (Barrientos et al. 2012; Yuen et al. 2012) were housed in the animal facility of School of Veterinary Medicine in the University of California, Davis (UC Davis), under specific pathogen-free conditions, at a controlled temperature of 22 ± 2°C and humidity of 50 ± 10%, with a cycle of 12 h light and 12 h dark. Animals were provided with Mouse Diet 20 (PicoLab) and autoclaved drinking water provided by UC Davis animal facility *ad libitum*. Well-trained, certified staff were responsible for the periodic breeding work to provide neonatal mice for primary cultures. All the animal related procedures met the requirements of the guidelines of Animal Use and Care of the National Institutes of Health and approved by the UC Davis Animal Use and Care Committee. The reagents used in this study are summarized in Table S1.

Primary Cortical Neurons Cultured from Neonatal Mice

Primary cultured neurons were used as a model reported to develop morphological (Cao et al. 2015) as well as functional changes that recapitulate several hallmarks of neurodevelopment observed *in vivo* (Feller 1999; Stafford et al. 2009). Procedures culturing cortical neurons from postnatal day 0 or 1 (both male and female) C57BL/6J WT and RyR1$^{T4826I/T4826I}$ knock-in mice were performed as described previously (Cao et al. 2011b). In brief, the dissociated cells were suspended in prewarmed neurobasal complete (NBC) medium [neurobasal medium supplemented with GS21 (2%, v/v), GlutaMAX (1%, v/v), 4-(2-hydroxyethyl)-1-piperazineethanesulfonic acid (HEPES; 10 mM)] containing 5% fetal bovine serum (FBS). Suspended cells were plated onto poly L-lysine (0.5 mg/mL in borate buffer) precoated 96-well imaging plate (BD Biosciences) at densities of 2,000; 75,000; and 130,000 cells/well for axonal and dendritic outgrowth, SCO, and microelectrode array (MEA) measurements, respectively. A final concentration of 5 μM of cytosine β-D-arabinofuranoside dissolved in FBS-free NBC was added at 24–30 h after plating. The neurons were maintained at 37°C with 5% CO_2 and 95% humidity until use at specified DIV.

Measurements of Intracellular Synchronous Ca^{2+} Oscillations

Intracellular Ca^{2+} dynamics in cultured neurons were measured as previously described (Cao et al. 2015). In brief, after incubation with the Ca^{2+} indicator Fluo-4/AM (4 μM) for 1 h, neurons were gently rinsed with prewarmed Locke's buffer (in mM: HEPES 8.6, KCl 5.6, NaCl 154, D-glucose 5.6, $MgCl_2$ 1.0, $CaCl_2$ 2.3, and glycine 0.1, pH 7.4) four times with a final volume of 175 μL per well. The plate was then loaded onto the imaging chamber of fluorescent imaging plate reader (FLIPR^{Tetra}, Molecular Devices). After an equilibration period of 5 min, SCO events were recorded for 120 s followed by the addition of vehicle [0.1% dimethylsulfoxide (DMSO)] or a defined concentration of DM (25 μL, 8× final concentration) using an automated, programmable pipetting system, and the fluorescent signals (F) were recorded for an additional 1,500 s at a sampling rate of 1 Hz. To measure the susceptibility to DM of cortical neurons at distinct development stages of *in vitro* cultures, the same batch neurons cultured in 96-well sister plates on 6, 8, 10, and 12 DIVs were used. To measure the developmental pattern of SCO in cortical neurons culture *in vitro*, Ca^{2+} dynamics were recorded for 600 s after an equilibration period of 5 min. The recordings were from the same batch of neurons cultured in 96-well sister plates on 2, 4, 6, 8, 10, and 12 DIVs. Half volume of the medium was changed with NBC at 4, 6, 8, 10, and 12 DIVs after recording the SCOs in the sister plates. For the subchronic exposure study, the cells were continuously treated with different concentrations of DM at 3 h postplating, and SCOs were recorded at 7 DIV. To compare the influence of RyR1 on SCO patterns and DM inhibition on SCO frequency and amplitude in both genotypes, paired cultures in the same 96-well imaging plate from WT and RyR1$^{T4826I/T4826I}$ pups were recorded simultaneously at 7 DIV. Data were presented as $\Delta F/F_0$, where F_0 is the minimal arbitrary fluorescence unit before addition. An event with amplitude $(\Delta F/F_0) > 0.15$ was considered to be an SCO. Peak amplitude and frequency were analyzed using Origin software (version 9.0; Origin Lab Corporation). SCO events recorded between 5 and 25 min after additions of test compound were analyzed to quantify DM effect on SCOs, since addition of fluid had an artificial disturbance on SCO pattern in the initial several minutes. Each experiment was repeated in at least three independent cultures. The averaged SCO frequency and amplitude from a culture were used as data points. The concentration–response curves of DM SCO response were fitted with a nonlinear logistic equation using Prism GraphPad software (version 7.0; GraphPad Software). One-way analysis of variance (ANOVA) followed by post hoc Bonferroni comparison were used to compare the statistical significance of SCO frequency and amplitude between different DIVs. *t*-Test was used to compare the statistical significance of SCO frequency and amplitude between WT and RyR1$^{T4826I/T4826I}$ neurons as well as the DM inhibition (percentage control of respective genotype) on SCO frequency and amplitude between two genotypes.

Measurements of Neuronal Electrical Spike Activity

Network ESA were recorded using 12-well MEA Maestro plates (Axion BioSystems) at 37°C as described previously (Cao et al. 2012b). MEA recording is an intact measurement that permits one to determine the ESA in the same population of neurons at different stages. Briefly, the 12-well Maestro plates with cortical neuron cultures at 5, 8, 11, and 14 DIVs were loaded onto a temperature-regulated head stage connected to a recording amplifier, and electric signals were acquired using AxIS software (Version 2.4, Axion BioSystems) for 15 min after an equilibration period of 5 min. Signals were acquired at a sampling frequency of 12.5 kHz and filtered using Butterworth Band-Pass filter (cutoff frequency of 200 Hz–3 kHz). The AxIS software was used to detect spontaneous events with a threshold of ≥8 times of the noise amplitude. NeuroExplorer software (version 4.0; NEX Technologies) was used to generate representative raster plot and the parameters such as number of active electrodes, spike frequency, burst frequency, and network burst frequency. DM exposure was initiated at 3 h postplating, and half-medium changes were conducted at 6, 9, and 12 DIVs with NBC containing the same concentrations of DM. Each experiment was repeated in at least three independent cultures, with four replicates per culture. The raw data of network activity was presented to reflect the developmental changes, and the DM responses in network activity in 5, 8, 11, and 14 DIVs were normalized to vehicle control (0.1% DMSO) obtained in respective DIVs. The averaged values of ESA parameters (spike frequency, burst frequency, and network burst frequency) from a culture were used as data points. Repeated measurements one-way ANOVA followed by post hoc Bonferroni comparison were used to compare the statistical significance of the ESA between two consecutive development DIVs. Ordinary two-way ANOVA followed by post hoc Bonferroni multiple comparison were used to determine the statistical significance between vehicle and DM-treated groups.

Immunocytochemistry and Morphometric Analysis

Immunocytochemistry was performed to visualize the morphology of neurons as previously described (Chen et al. 2017). The genesis of axonal growth has been demonstrated by 1 DIV and dendritic arbor formation manifests by 5 DIV (Cáceres et al. 1986; Dotti et al. 1988). Cortical neurons cultured in 96-well imaging plates were exposed to defined concentration (3 nM–1,000 nM) of DM from 3 h after plating. The neurons were fixed with 4% paraformaldehyde for 10 min at 2 and 7 DIVs for axonal growth and dendritic complexity analysis, respectively. After washing with PBS (4 × 5 min each), the cells were permeabilized with 0.25% Triton X-100 for 5 min followed by blocking with 10% goat serum for 1 h. After washing with PBS (4 × 5 min each), cells were then incubated with anti-MAP-2B primary antibody (1:2000) in PBS containing 10% goat serum overnight at 4°C. Cells were washed with PBS (4 × 5 min each) and then incubated with Alexa Fluor® 488–conjugated goat anti-chicken secondary antibody (1:500) for 1 h at room temperature. Pictures were recorded using an ImageXpress® High Content Imaging System (Molecular Devices) using a 10 × objective with fluorescein isothiocyanate filter. The ImageXpress® High Content Imaging System was able to compartmentalize each well to different zones and capture the pictures in each zone by imputing the parameters of a 96-well plate. Nine adjacent sites (3 × 3), which cover ~60% of the center surface area, were pictured for each well. The longest neurite that exceeded three times the length of the cell body (soma) was counted as an axon. Images digitized at 8-bit were used to manually trace axons and length using Image J software (version 1.49s; U.S. National Institutes of Health) with Neuron J Plugin as previously described (Meijering et al. 2004). An axon was continuously traced from the edge of the cell body until the fluorescence signal/background noise ratio was <1.2. Image J software was used for Sholl analysis (Ferreira et al. 2014) with rings set at 5-pixel increments from the soma (1 pixel = 0.65 μm). In brief, after exporting the image to Image J, the center of individual neurons was defined, and the numbers of intersections at each ring with different distance to soma were counted using a macro, as described previously (Torres-Espin et al. 2014). Each experiment was repeated on at least two independent cultures, with at least three wells in each culture. Axonal length and mean value of intersections of each neuron were used to determine the *n* value, as described in previous papers (Kaplan et al. 2017; Mukai et al. 2015). One-way ANOVA followed by post hoc Bonferroni comparison was used to compare the statistical significance between vehicle- and DM-exposed groups. To assess the influence of sample size in the analysis, a randomly subsampling strategy was used. Specifically, an equal number of samples were randomly chosen from each group for 100 times, and the ANOVA test with Bonferroni correction was performed at each subset using R package software (version 3.4.1; R Development Core Team). Statistical significance between WT and $RyR1^{T4826I/T4826I}$ neurons and DM response was performed using two-way ANOVA.

Preparation of RyR1 and RyR2 from Muscle and Mixed RyRs from Brain

A junctional SR membrane fraction enriched in RyR1 was isolated from fast-twitch skeletal muscles of <1-y-old male (~3 kg) New Zealand White rabbits (Charles River Laboratories), as previously described (Pessah et al. 1985; Saito et al. 1984). Briefly, ground skeletal muscle was homogenized, and membrane fractions were separated with differential centrifugation to obtain a crude membrane fraction that was further purified by sucrose-density gradient centrifugation overnight to harvest the junctional sarcoplasmic reticulum membrane fraction enriched in RyR1. The fractions between 38–45% sucrose layers were collected, pooled, spun-down, resuspended, and stored at −80°C until use. A cardiac microsomal preparation enriched in RyR2 and a brain cortical homogenate containing a mixture of all three isoforms of RyR1, RyR2, and RyR3 (Berridge 2014) were prepared from WT C57BL/6J mice (3–6 months old), as described previously (Berridge 2014; Feng et al. 2017; Wong et al. 1997; Zimanyi and Pessah 1991). To obtain microsomal homogenates, ground cardiac tissue was suspended and subjected to two sequential bursts of 30 s each at 23,000 rpm using a PowerGen 700D (Fisher Scientific); ground brain cortical tissue was suspended and homogenized using a Potter-Elvehjem tissue grinder (VWR) for 30 s, repeated three times, in a 30-s interval between two homogenizations. Homogenates were then centrifuged at 1,000 rpm for 30 s, and the supernatant was collected and further centrifuged 110,000 × *g* for 1 h at 4°C. The pellets were collected and resuspended, and stored at −80 °C. Protein concentrations were determined using the DC™ protein assay kit.

Equilibrium [^{3}H]Ry Binding Analysis

Equilibrium binding analyses of [^{3}H]Ry to skeletal muscle RyR1 (0.05 mg/mL), cardiac muscle RyR2 (0.5 mg/mL), and brain cortical homogenates (0.5 mg/mL) were measured at 37°C for 3 h with constantly shaking in a binding buffer consisting of 250 mM KCl, 14 mM NaCl, 20 mM HEPES, pH 7.4, and 2 μM free Ca^{2+} (obtained by the addition of egtazic acid calculated using the software bound and determined (Brooks and Storey 1992). The concentrations of [^{3}H]Ry (specific activity: 56.6 Ci/mmol; PerkinElmer) were used at 1 nM, 2 nM, and 10 nM for skeletal, cardiac, and brain preparations, respectively. Nonspecific [^{3}H]Ry binding was measured in the presence of a 1,000-fold of unlabeled ryanodine. Samples were harvested by rapid filtration through Whatman GF/B glass fiber filters (Whatman) using a 48-sample cell harvester (Brandel) to wash three times with 5 mL of ice-cold buffer containing (in mM) 250 KCl, 14 NaCl, 20 HEPES, and 2 μM Ca^{2+}, pH 7.4. [^{3}H]Ry remained on filters was quantified using a Beckman scintillation counter (Model LS6500, Beckman). Experiments were repeated in three independent preparations with three replicates each, and the data was presented as mean ± standard error of the mean (SEM). The DM concentration–response curves were fitted with a nonlinear logistic equation using Prism GraphPad software.

Single-Channel Voltage Clamp

Bilayer lipid membranes (BLM) were formed by mixing of 30 mg/mL phosphatidylethanolamine, phosphatidylserine, and phosphatidylcholine in *n*-decane. RyR1 channel incorporation into BLM was accomplished by induced vesicle fusions with BLM, as previously described (Holland et al. 2017). The recording buffer used was 500 mM (*cis*-cytoplasmic side) and 50 mM (*trans*-luminal side) CsCl, buffered with 20 mM HEPES, pH 7.4, to establish a 10:1 Cs^+ gradient. Fluctuations in channel current were recorded at a holding potential of −40 mV applied to the *trans* side. DMSO (0.1%) as vehicle control and DM was sequentially added to the *cis* to reach the final concentrations of 10 and 30 nM. Baseline (control) was recorded for 1–1.5 min before the extended time course of 3–15 min in the presence of DM. Data acquisition was made using digitizer DD1440A (Molecular Devices), digitized at 10 kHz and filtered with 1-kHz low-pass filter (8-pole low-pass Bessel filter; Warner Instruments). Data analysis was performed using Clampfit 10.4 (Molecular Devices) for channel open probability (P_o), mean open time (τ_o), and mean closed time (τ_c). Statistical significance between groups was calculated by one-way ANOVA followed by post hoc Bonferroni comparison. The data were from three independent single-channel recordings, and

the changes in P_o, τ_o, and τ_c were normalized to their respective controls of each channel.

MTT Assay

Neocortical neurons cultured in 96-well plate at 7 DIV were used to measure the cell viability using 3-(4,5-dimethylthiazol-2-yl)-2,5-triphenyl tetrazolium bromide (MTT) assay, as described previously (Zheng et al. 2019). Briefly, after washing with Locke's buffer, neurons were exposed to vehicle (0.1% DMSO) or Fluo-4/AM (4 μM) in the Locke's buffer for 1.5 h. The Locke's buffer was replaced with Neuronbasal Complete medium and incubated in a CO_2 incubator for additional 24 h. After aspirating the medium, a volume of 100 μL medium containing 0.5 mg/mL MTT was added to each well and incubated for 10 min at 37°C. After discarding the medium, a volume of 150 μL DMSO was added to each well. The absorbance was measured at 570 nm and 650 nm in a microplate reader (Tecan Group Ltd.) to measure the content of formazan generated in each well. The data were presented as mean ± SEM. A *t*-test was used to analyze the statistical significance between Fluo-4/AM and vehicle groups.

Preparation of Cis-(2,2-Dibromovinyl)-2,2-Dimethylcyclopropane-1-Carboxylic Acid

A total of 20 mg of DM was dissolved in 6 mL of methanol and mixed with 400 μL of 10% NaOH. The DM was hydrolyzed by incubating the mixture at room temperature for 2 h. The reaction products were subjected to reverse-phase high-performance liquid chromatography on an Xtimate® C18 column (10 × 250 mm; Welch Tech.) eluted with 72% of methanol with a flow rate of 2 mL/min for purification. One of hydrolytic metabolites, *Cis*-(2,2-dibromovinyl)-2,2-dimethylcyclopropane-1-carboxylic acid (*cis*-DBCA) (Retention time, $t_R = 22.5$ min) was purified, and the structure was confirmed by NMR.

Statistical Analyses

All data were expressed as mean ± SEM and graphed using Prism GraphPad software. Statistical analysis was performed with appropriate comparisons described in each "Methods" section with Prism GraphPad software. A $p < 0.05$ was considered to be statistically significant.

Results

Developmental Patterns of Synchronous Ca^{2+} Oscillations and Electrical Spike Activity

A recent study reported that Fluo-4/AM suppressed the ouabain-sensitive Na^+–K^+ adenosine triphosphate activity, leading to neuron death (Smith et al. 2018). We therefore first examined the viability of primary cultured cortical neurons after exposure to Fluo-4/AM. Fluo-4/AM (4 μM) had no effect on the neuronal viability ($p = 0.97$) under our experimental conditions (see Figure S1). Cortical neurons harvested from mice pups at postnatal day 0 to 1 and grown on 96-well plates at a density of 75,000 cells/well displayed distinctive patterns of SCO activity during the developmental window investigated (2 to 12 DIVs) (Figure 1A,B). SCO frequency significantly increased during *in vitro* development ($F = 21.16$; degrees of freedom $(DF) = 5$; $p < 0.0001$) (Figure 1C). Specifically, there was insufficient synapse formation to drive detectable network SCO activity at 2 DIV. By 4 DIV, SCOs were apparent (mean frequency of 0.93 ± 0.04 SCOs/min) and continued to gradually increase between 4 and 12 DIV, reaching 3.6 ± 0.21 SCOs/min by 12 DIV (Figure 1C). SCO amplitude also significantly changed during *in vitro* development ($F = 5.94$; $DF = 5$; $p = 0.005$) (Figure 1C). Neuronal networks displayed a temporal increase in Ca^{2+} transient amplitude between 4 DIV (0.68 ± 0.01) and 6 DIV (1.1 ± 0.29), which gradually declined at longer DIV (Figure 1C).

Cortical neurons grown on MEA exhibited spontaneous ESAs that increased between 5 and 14 DIV (Figure 2). The number of electrodes recording ESAs ($F = 25.12$; $DF = 3$; $p = 0.03$), mean spike frequency ($F = 9.43$; $DF = 3$; $p = 0.01$), burst frequency ($F = 6.02$; $DF = 3$; $p = 0.02$), and network burst frequency ($F = 6.67$; $DF = 3$; $p = 0.02$) all significantly increased with *in vitro* development (Figure 2C–F). At 5 DIV, 7.7 ± 3.4% electrodes displayed measurable spike discharges that gradually increased to 49.8 ± 10.2% at 14 DIV (Figure 2C). The average spike frequency of active electrodes at 5 DIV was 2.51 ± 1.19 spikes/s, and at 14 DIV reached 246.10 ± 80.56 spikes/s (Figure 2D). Beginning at 8 DIV, clusters of ESA (termed bursts) were detected, and their number gradually increased with neuron development, from 0.79 ± 0.32 bursts/s at 8 DIV to 9.30 ± 3.53 bursts/s at 14 DIVs (Figure 2E). Network burst frequency represented a measure of the synchronicity (Vardi et al. 2016) of events detected across the electrode array. Network bursting events were detected beginning at 8 DIV and increased tenfold by 14 DIV (Figure 2F).

Influence of Acute Nanomolar Deltamethrin Exposure on Synchronous Ca^{2+} Oscillation Patterns

We next investigated the acute effects of nanomolar DM exposure at 6, 8, 10, and 12 DIVs to determine how it influenced ESA parameters described above over the development *in vitro*. DM exposure rapidly suppressed SCO amplitude and frequency in a concentration-dependent manner, and the degree was dependent on the stage of development of the neuronal network (Figure 3). The half-maximal inhibitory concentration (IC_{50}) values for DM

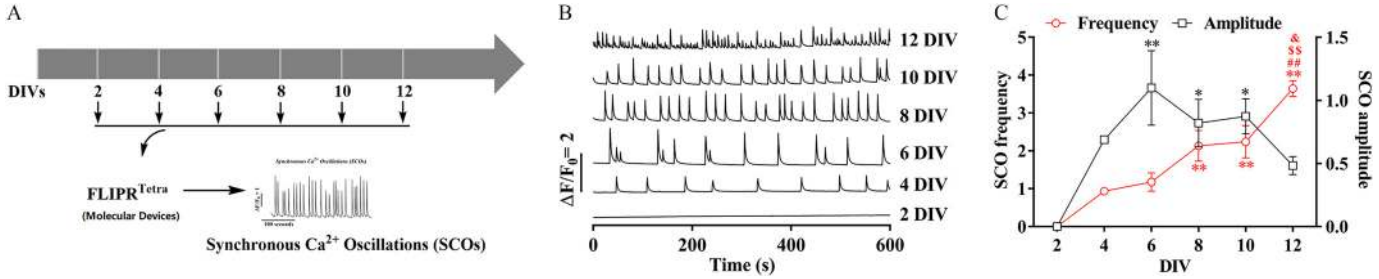

Figure 1. Developmental patterns of SCOs in primary cortical neurons. (A) Schematic diagram outlining the measurement of SCO development changes in cultured cortical neuronal networks. (B) Representative traces of SCOs recorded from primary cortical neuronal network at 2, 4, 6, 8, 10, and 12 DIVs. (C) Quantification of the SCO frequency and amplitude at different developmental stages. The mean value of each plate was used as analysis unit. Each data point represents the mean ± standard error of the mean (SEM) from three independent cultures. One-way analysis of variance (ANOVA) followed by post hoc Bonferroni comparison was used to compare the statistical significance of SCO frequency and amplitude between different DIVs. Note: DIV, days *in vitro*; SCO, synchronous Ca^{2+} oscillations. $^*p < 0.05$; $^{**}p < 0.01$ vs. 2 DIV; $^{\#\#}p < 0.01$ vs. 4 DIV; $^{\$\$}p < 0.01$ vs. 6 DIV; $^{\&}p < 0.05$ vs. 8 DIV.

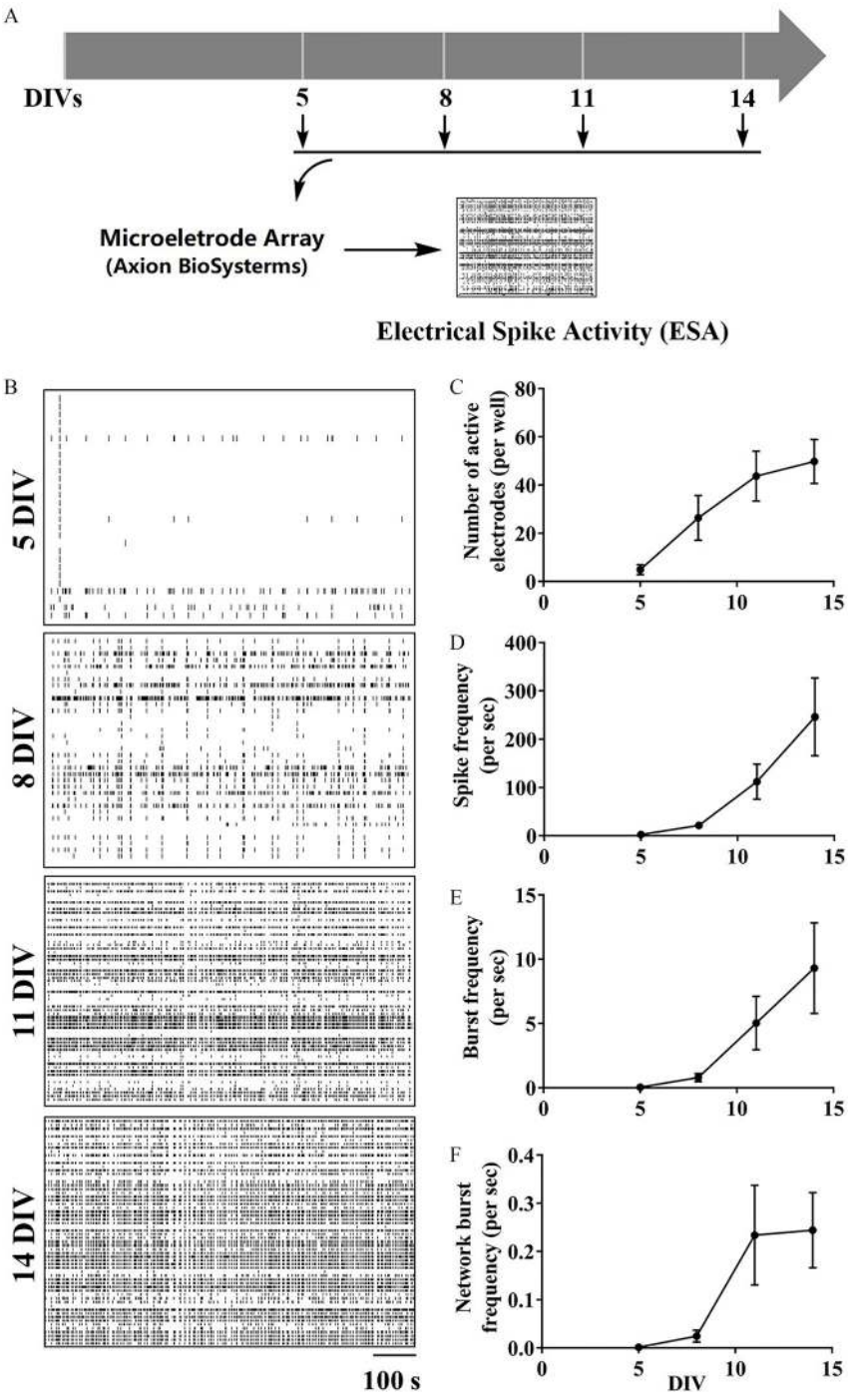

Figure 2. Developmental patterns of ESA in primary cortical neurons. (A) Graphical paradigm outlining the measurement of ESA development changes in cultured cortical neuronal networks. (B) Representative raster plots of ESA in the same neuronal cultures at 5, 8, 11, and 14 DIVs. (C–F) Quantification of the number of (C) active electrodes, (D) spike frequency, (E) burst frequency, and (F) network burst frequency in neuronal cultures at different DIVs. The mean value of each plate was used as the analysis unit. Each data point shown in (B–E) represents the mean ± standard error of the mean (SEM) from three independent cultures. Repeated measurements one-way analysis of variance (ANOVA) analysis was used to analyze the number of active electrodes, spike frequency, burst frequency, and burst frequency during *in vitro* development. No statistical significance was observed between two different DIVs when using post hoc Bonferroni comparison. Note: DIV, days *in vitro*; ESA, electrical spike activity.

suppressing SCO amplitude quantified between 5 and 25 min after addition of DM were 37.6 nM [95% confidence interval (CI): 22.5, 62.3], 21.3 nM (95% CI: 13.6, 33.4), 29.8 nM (95% CI: 20.3, 43.5), and 78.1 nM (95% CI: 26.2, 222.2) at 6, 8, 10, and 12 DIVs, respectively (Figure 3B, right panel; Table 2). The maximal suppression of SCO amplitude by DM was highly dependent on neuronal development stages *in vitro*. At 6 DIV, DM could completely suppress SCO activity, whereas incomplete suppression of SCO amplitude was observed as the neuronal networks developed (Figure 3B, right panel; Table 2). The maximal suppression of SCO amplitude at 8, 10, and 12 DIVs were 88.2% (95% CI: 80.0, 97.2), 67.8% (95% CI: 61.9, 74.1), and 60.5% (95% CI: 43.8, 85.5), respectively. DM also decreased SCO frequency at 6 and 8 DIVs [IC_{50} 139.6 nM (95% CI: 73.0, 262.9) and 190.8 nM (95% CI:

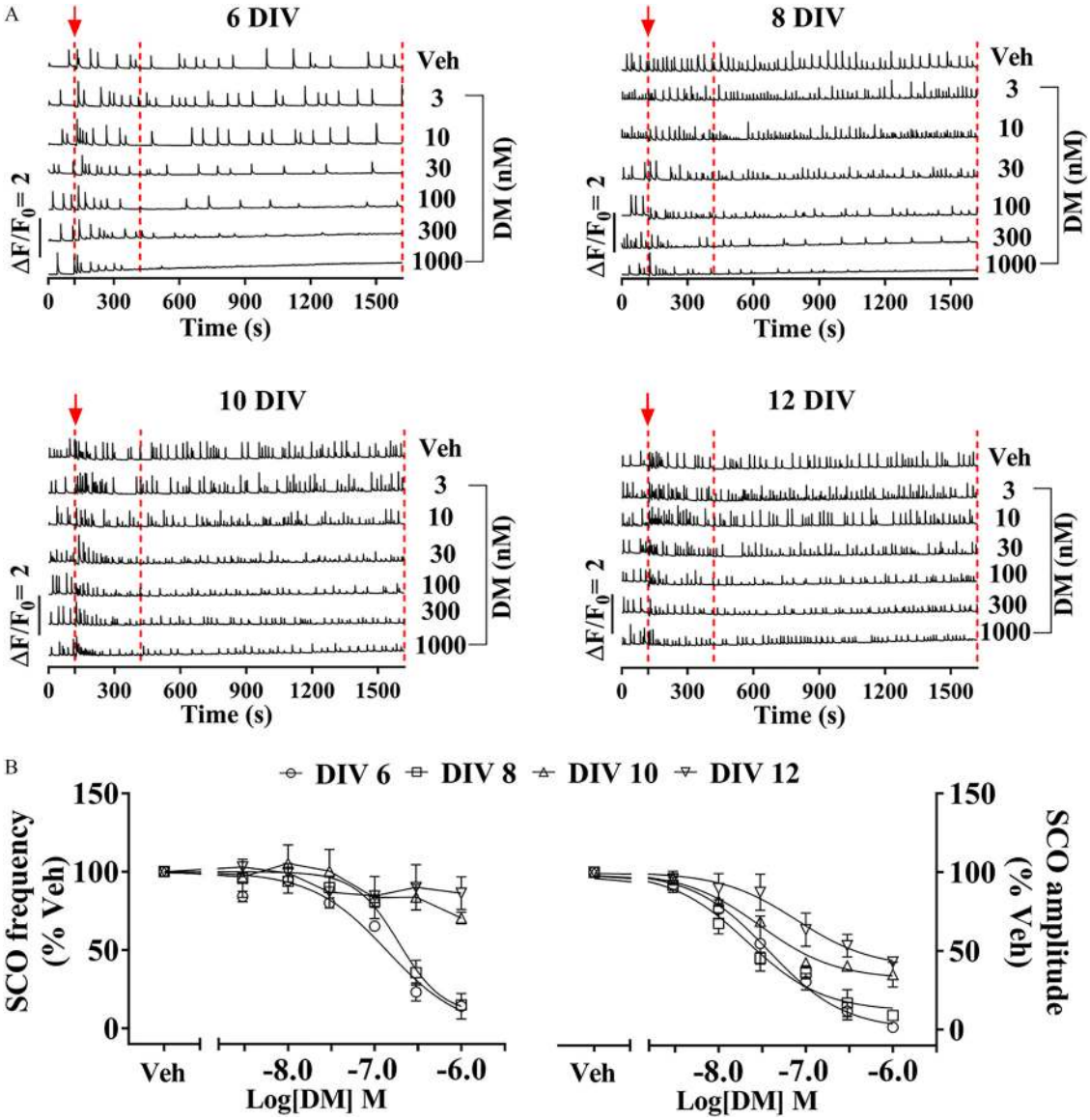

Figure 3. Acute effect of DM on SCO patterns at specified DIVs. (A) Representative traces of SCOs measured at 6, 8, 10, and 12 DIVs neurons cultured in 96-well sister plates. Arrowhead together with the dashed line at 120 s indicate the addition of Veh (0.1% DMSO) or different concentrations of DM. Two additional dashed lines indicate the time frame that was used to quantify the SCO frequency and amplitude. (B) Concentration–response relationship for DM-altered SCO frequency (left panel) and SCO amplitude (right panel). The mean value of SCO frequency and amplitude from each plate was used as analysis unit. Each data point represents the mean ± standard error of the mean (SEM) from four independent cultures. The concentration–response curves of DM SCO response were fitted with a nonlinear logistic equation using Prism GraphPad software. The half-maximal inhibitory concentration (IC_{50}) values and maximal inhibition of DM at distinct DIVs are summarized in Table 2. Note: DIV, days *in vitro*; DM, deltamethrin; DMSO, dimethylsulfoxide; SCO, synchronous Ca^{2+} oscillations.

126.4, 1,471.0), respectively]. At 10 and 12 DIVs, the maximal inhibition achieved at 1 μM DM was only 29.5 ± 3.7% and 13.6 ± 10.4%, respectively (Figure 3B, left panel; Table 2). By comparison, the two major DM hydrolytic metabolites, 3-PBA and *cis*-DBCA, altered neither SCO frequency nor amplitude in 8 DIV cortical neurons (F = 0.13; DF = 6; $p = 0.99$) (Figure S2). This was consistent with the previous demonstration that 3-PBA did not affect the viability of SH-SY5Y cells, even at 100 μM (Romero et al. 2012).

Table 2. Relative potency and maximum inhibition of acute DM exposure on SCO parameters at different DIVs.

	SCO frequency		SCO amplitude	
DIVs	IC_{50} (nM) (95% CI)	Max. inhib. (%) (95% CI)	IC_{50} (nM) (95% CI)	Max. inhib. (%) (95% CI)
6	139.6 (73.0, 262.9)	100.0 (82.9, 124.7)	37.6 (22.5, 62.3)	100.0 (88.6, 112.7)
8	190.8 (126.4; 1,471.0)	90.9 (73.6, 206.8)	21.3 (13.6, 33.4)	88.2 (80.0, 97.2)
10	N.D.	29.5 ± 3.7[a]	29.8 (20.3, 43.5)	67.8 (61.9, 74.1)
12	N.D.	13.6 ± 10.4[a]	78.1 (26.2, 222.2)	60.5 (43.8, 85.5)

Note: The half-maximal inhibitory concentration (IC_{50}) values and maximum inhibition were obtained by fitting the data in Figure 3B with a nonlinear logistic equation using Prism GraphPad software. CI, confidence interval; DIV, days *in vitro*; DM, deltamethrin; Max. inhib., maximal inhibition; SCO, spontaneous Ca^{2+} oscillations; N.D., not determined.
[a]Since the data obtained from 10 and 12 DIV did not permit curve fitting, the maximal inhibition was reported at 1 μM DM.

Influences of Subchronic Deltamethrin Exposure on Network Synchronous Ca^{2+} Oscillation and Electrical Spike Activity Patterns

Cortical neurons were exposed to vehicle or defined concentrations of DM beginning 3 h after cell plating and SCO patterns were measured on 7 DIV with FLIPR^{Tetra} (Molecular Devices). Subchronic exposure to DM decreased the SCO frequency on 7 DIV relative to vehicle control [IC_{50} of 61.1 nM (95% CI: 29.1, 130.4)], although suppression was incomplete at the highest DM concentration tested (Figure 4A,B). Unlike acute exposure to DM shown in Figure 3, subchronic DM did not reduce SCO amplitude, but rather produced a negligible trend toward SCO augmentation that was not statistically significant (Figure 4B).

Cortical neurons plated on MEA were exposed to DM (10 and 30 nM) beginning 3 h postplating to assess influences on ESA patterns at specified DIVs (Figure 5). DM exposure significantly affected both spike frequency ($F = 44.52$; $DF = 2$; $p < 0.0001$) and burst frequency ($F = 11.88$; $DF = 2$; $p = 0.0002$) but not network burst frequency ($F = 0.20$; $DF = 2$; $p = 0.82$) (Figure 5B–E). At 5 DIV, DM (30 nM) significantly reduced spike frequency and ESA burst by $62.5 \pm 10.1\%$ ($p < 0.01$), and $55.0 \pm 9.5\%$ ($p < 0.01$), respectively (Figure 5B–D). These inhibitory effects of DM on spike frequency persisted through 14 DIV. However, the magnitude of DM-suppressed spike frequency declined as neuronal networks developed *in vitro* (Figure 5C). By 14 DIV, subchronic DM exposure had no significant influence on burst frequency compared with control (Figure 5D). Although we observed spike activity and burst firing as early as 5 DIV, network bursts occurred starting at 8 DIV (Figure 5E). Subchronic exposure to DM (10 or 30 nM) was without effect on the frequency of network bursts (Figure 5E).

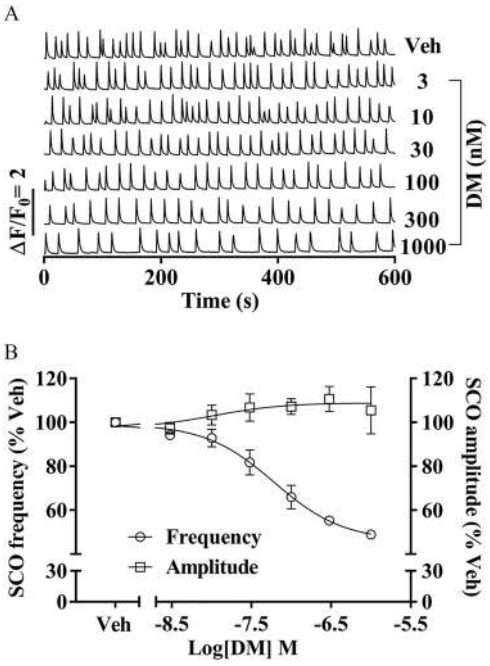

Figure 4. Influence of subchronic DM exposures on SCO patterns. (A) Representative traces of SCOs measured at 7 DIV. Neurons were continuously exposed to Veh (0.1% DMSO) or different concentrations of DM starting from 3 h after plating. (B) Concentration–response relationships for DM altered SCO frequency and amplitude. The mean value of each plate was used as analysis unit. Each data point represents the mean ± standard error of the mean (SEM) from three independent cultures. The concentration–response curves of DM SCO response on frequency and amplitude were fitted with a nonlinear logistic equation using Prism GraphPad software. Note: DIV, days *in vitro*; DM, deltamethrin; DMSO, dimethylsulfoxide; SCO, synchronous Ca^{2+} oscillations; Veh, vehicle.

Influence of Deltamethrin on Axonal and Dendritic Outgrowth

Considering the significant influences of DM on SCO and ESA patterns on neuronal networks *in vitro*, we posited that subchronic DM would influence morphometric properties of neuronal axonal growth and dendritic complexity. DM (3–1,000 nM) exposure, commencing 3 h after plating and continuing for 48 h and 7 d, was used to investigate the axon elongation and dendritic arborization, respectively. Vehicle (0.1% DMSO) treatment for 48 h had no effect on the axonal growth (Figure S3A,B). In contrast, DM exposure significantly affected axonal outgrowth ($DF = 6$; $F = 17.59$; $p < 0.0001$) and produced a nonmonotonic concentration–effect relationship on axonal elongation (Figure 6). Cells treated with 10 and 30 nM DM had significantly longer axons (by $10.4 \pm 1.3\%$; $p < 0.01$; and $16.1 \pm 2.0\%$; $p < 0.01$, respectively) compared with vehicle-treated cells. The maximal axonal length was observed in the presence of 100 nM DM ($20.9 \pm 1.9\%$; $p < 0.01$) (Figure 6C). Power analysis also showed the minimum sample sizes needed for detecting significant differences among treatment groups were 200, 130, and 300 neurons for 30, 100, and 300 nM DM, respectively (Figure S4). Vehicle (0.1% DMSO) treatment had no effect on neuron complexity (Figure S3C–E). However, neuronal cultures exposed DM (100 nM and 300 nM) under these conditions exhibited higher complexity that was dependent on the radius of the circles used in the Sholl analysis (Figure 6D–E). DM significantly affected the number of intersections at radius of 30 pixels ($DF = 5$; $F = 6.12$; $p < 0.0001$) and 60 pixels ($DF = 5$; $F = 8.16$; $p < 0.0001$), respectively (Figure 6F). At a radius of 30 pixels, the numbers of intersections were significantly higher by $13.3 \pm 1.7\%$ ($p < 0.05$) and $23.3 \pm 3.3\%$ ($p < 0.01$) in the presence of 100 nM and 300 nM of DM, respectively, compared with vehicle-treated cells. At a radius of 60 pixels, the number of intersections were significantly higher by $28.6 \pm 7.0\%$ ($p < 0.05$) and $30.1 \pm 10.1\%$ ($p < 0.05$), respectively (Figure 6F). Lower concentrations of DM had no effect on dendritic complexity of cortical neurons under these experimental conditions (Figure 6F).

Influence of Deltamethrin on Ryanodine Receptor Function

We further examined the mechanisms by which DM altered RyR function that was previously identified as a potential target of DM (Morisseau et al. 2009) using radioligand binding assay and single-channel lipid bilayer recording. Binding of [^{3}H]Ry to RyR1 and RyR2 was higher at DM concentrations >3 μM than with vehicle (Figure S5). In the skeletal muscle and cardiac muscle preparations, the maximal response reached 258.2% (95% CI: 240.4, 279.9) and 164.8% (95% CI: 147.7, 199.6) of respective vehicle (0.1% DMSO) controls (Table S2). Similarly, in the preparations derived from cortex, which expressed all three RyR isoforms (Feng et al. 2017), [^{3}H]Ry binding was higher in the presence of DM, with a maximal increment of 239.5% (95% CI: 198.6, 294.8) of control (Figure S5; Table S2).

DM also altered the pattern of RyR1 single-channel gating kinetics in voltage clamp recordings (Figure 7A–C). DM significantly affected mean closed time ($DF = 2$; $F = 166.3$; $p < 0.0001$), τ_o, ($DF = 2$; $F = 147.0$; $p < 0.0001$), and open probability ($DF = 2$; $F = 24.77$; $p < 0.0025$) (Figure 7D). DM at 10 nM and 30 nM significantly decreased the RyR1 channel τ_c to $25.1 \pm 10.1\%$ ($p < 0.01$) and $4.1 \pm 3.9\%$ ($p < 0.01$) of control (Figure 7D). The τ_o was also significantly increased to 2.35 ± 0.09 folds ($p < 0.01$) of control after addition of DM (30 nM), while 10 nM of DM had no measurable (significant) increase in τ_o (Figure 7D). DM at 30 nM dramatically increased the open probability (P_o) of RyR1 channel to 36.2 ± 12.7 folds of control ($p < 0.01$) (Figure 7D).

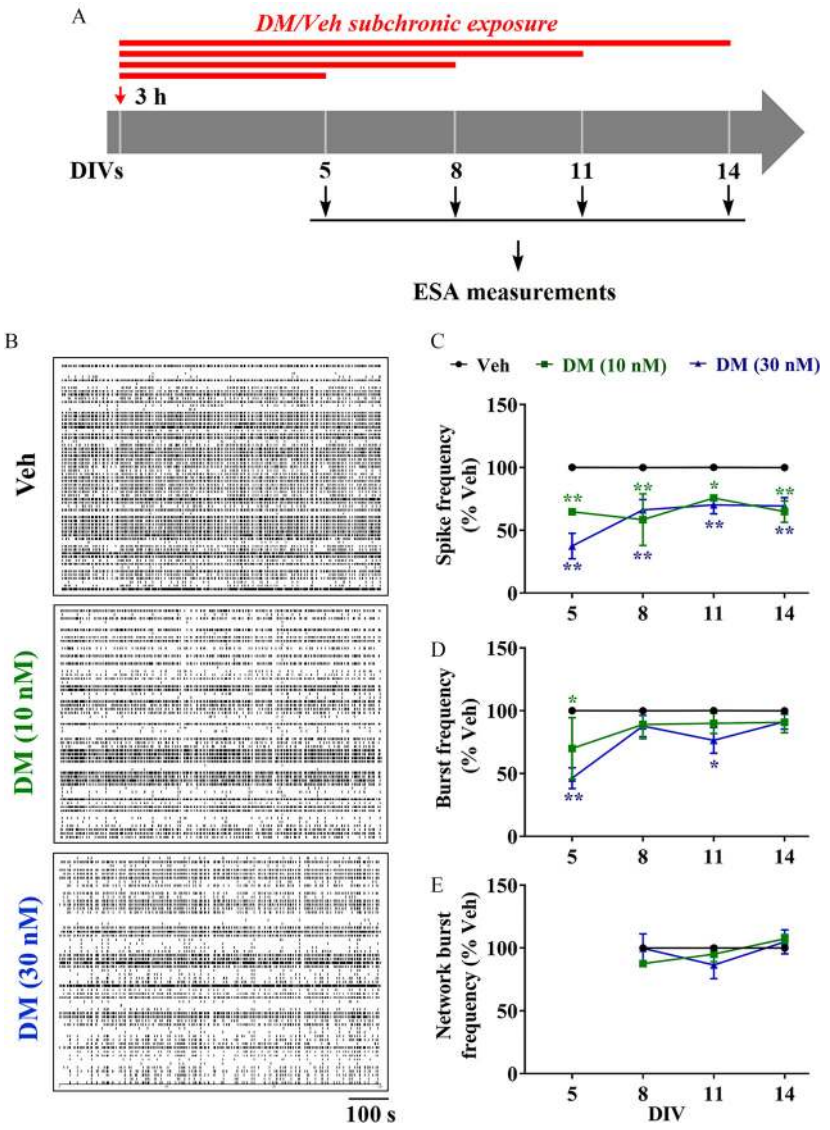

Figure 5. Influence of subchronic DM exposures on patterns of ESA. (A) Graphical paradigm outlining subchronic DM exposure for ESA measurement. Neurons were continuously exposed to Veh (0.1% DMSO) or 10 or 30 nM DM commencing 3 h after plating, and ESA was recorded at 5, 8, 11, and 14 DIVs. (B) Representative raster plots of ESA recorded on cortical neurons at 5, 8, 11, and 14 DIVs. (C–E) Quantification of (C) spike frequency, (D) burst frequency, and (E) network burst frequency in the same neuronal cultures at different DIVs. The mean value of each plate was used as analysis unit. Each data point represents the mean ± standard error of the mean (SEM) from four independent cultures. Two-way analysis of variance (ANOVA) followed by post hoc Bonferroni multiple comparison was used to determine the statistical significance between Veh and DM-treated groups. Note: DIV, days *in vitro*; DM, deltamethrin; DMSO, dimethylsulfoxide; Veh, vehicle. $*p < 0.05$; $**p < 0.01$ vs. Veh at respective DIVs.

Susceptibility to Deltamethrin between Wild-Type and RyR1$^{T4826I/T4826I}$ Neurons

Given that DM suppressed SCO frequency and amplitude at 6 DIV neurons with IC_{50} values of 139.6 nM and 37.6 nM, respectively, we selected an intermediate concentration of DM (100 nM) to investigate the possible influence of DM on SCOs on the neurons cultured from mice expressing an RyR1 gain-of-function knock-in mutation (RyR1$^{T4826I/T4826I}$). The SCO frequency in neurons expressing RyR1$^{T4826I/T4826I}$ was comparable with that measured in neurons cultured from C57BL/6J (WT) mouse pups (Figure 8A, B). However, the SCO amplitude in RyR1$^{T4826I/T4826I}$ neurons was significantly smaller ($10.7 \pm 4.9\%$; $p < 0.05$) than that measured in WT neurons (Figure 8A,B). RyR1$^{T4826I/T4826I}$ neurons exhibited a greater SCO response to DM exposure. DM (100 nM) treatment inhibited SCO frequency by $58.9 \pm 11.9\%$ in RyR1$^{T4826I/T4826I}$ cortical neurons, whereas in WT cortical neurons, the inhibition was $11.0 \pm 14.4\%$ ($p < 0.01$) (Figure 8D). Similarly, inhibition of SCO amplitude was greater in RyR1$^{T4826I/T4826I}$ cortical neurons ($73.2 \pm 5.4\%$) compared with that in WT neurons ($61.0 \pm 2.1\%$) ($p < 0.05$) (Figure 8D).

Effects of RyR1$^{T4826I/T4826I}$ Mutation on Deltamethrin-Induced Axon Growth

The possible influence of RyR1$^{T4826I/T4826I}$ on axon growth and susceptibility to DM exposure was further investigated using the cortical neuronal culture model. Axonal length in RyR1$^{T4826I/T4826I}$ neurons was significantly longer (203.3 ± 6.2 μm) than that in WT neurons (159.7 ± 4.7 μm; $p < 0.01$) at 2 DIV (Figure 9A,B). RyR1$^{T4826I/T4826I}$ cortical neurons treated with DM at 100 nM had significantly ($p < 0.01$) longer mean axon length (Figure 9A,B).

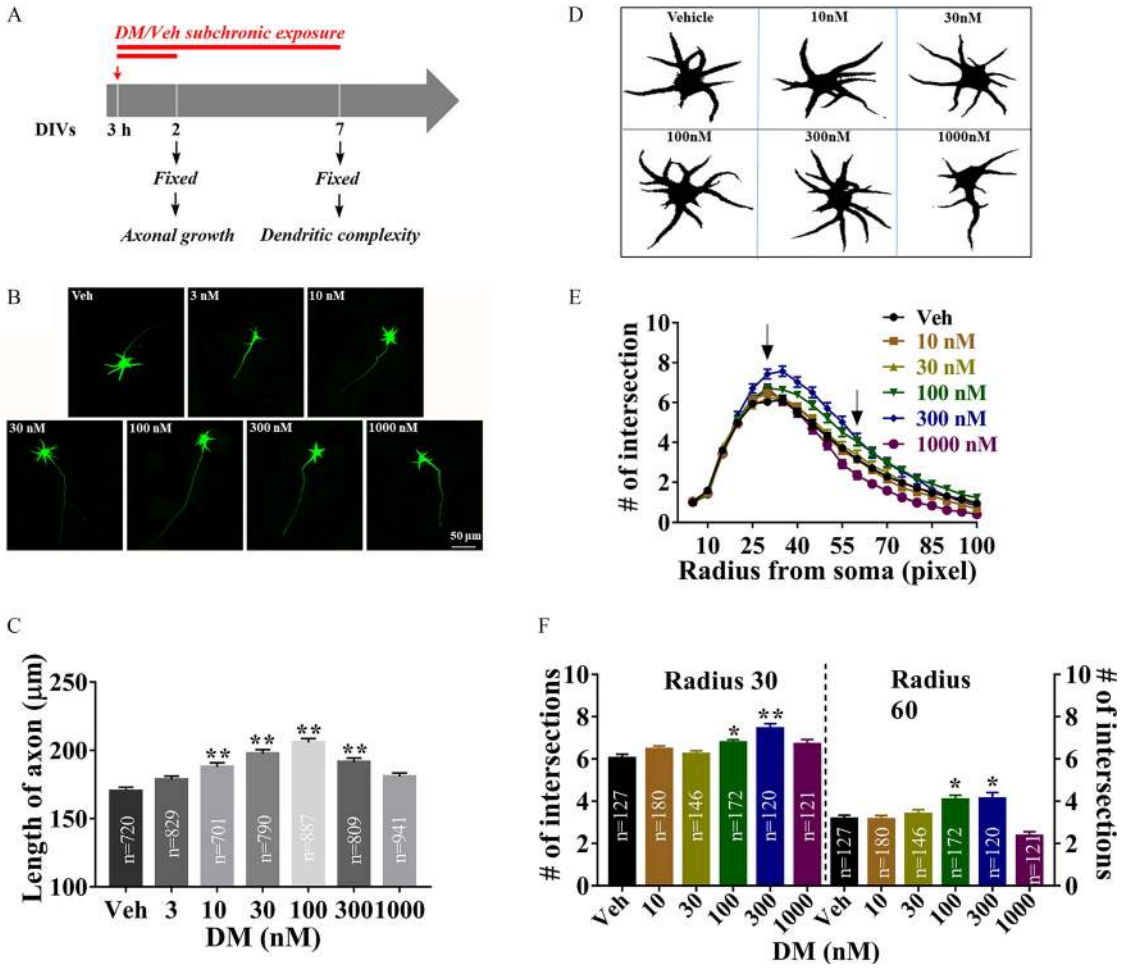

Figure 6. Subchronic effect of DM exposure on axonal and dendritic outgrowth. (A) Graphical paradigm outlining subchronic exposure of DM for axonal and dendritic outgrowth. (B) Representative images of neurons exposed to Veh (0.1% DMSO) and different concentrations of DM commencing 3 h after plating and immunostained with MAP-2B antibody at 2 DIV. (C) Quantification of the axon length in the absence and presence of DM exposure. (D) Image J–processed representative images of neuronal morphology immunostained with MAP-2B at 7 DIV. Neurons were continuously exposed to Veh (0.1% DMSO) or different concentrations of DM starting from 3 h after plating. (E) Quantification of numbers of intersections at different radius in the absence and presence of DM exposure. The number of intersections was plotted with different radius (pixels). (F) Quantification the dendritic complexity after DM exposure. The radii of 30 and 60 pixels were chosen to quantify the number of intersections. The total number of neurons tested was inserted in the bar graph, and axonal length and number of intersections of each neuron was used as analysis unit. Each data point represents the mean ± standard error of the mean (SEM) from three independent cultures. One-way analysis of variance (ANOVA) followed by post hoc Bonferroni comparison was used to compare the statistical significance between Veh and DM exposed groups. Arrowheads indicate the radii of 30 and 60 pixels, respectively. Note: DIV, days *in vitro*; DM, deltamethrin; DMSO, dimethylsulfoxide; Veh, vehicle. $*p < 0.05$; $**p < 0.01$ vs. Veh. Bar = 50 µm.

RyR1$^{T4826I/T4826I}$ neurons treated with DM (30 and 100 nM) exposure also displayed longer axon length compared with that in WT neurons with respective DM treatment ($p < 0.01$ and $p < 0.05$, respectively) (Figure 9A,B).

Discussion

Primary cultured cortical neurons recapitulate several neurodevelopmental and functional hallmarks of neurodevelopment observed *in vivo* (Feller 1999; Stafford et al. 2009). This culture system displays a variety of intrinsic signaling pathways that are essential to the development and consolidation of the neuronal network (George et al. 2012). During development, dendritic arborization, axonal elongation, and synapse formation form an extensive neuronal network (George et al. 2012), displaying spontaneous ESA (Frega et al. 2012) and SCOs (Cao et al. 2012a; Cao et al. 2014b), two interrelated and essential biological processes that affect neuronal network refinement (Feller 1999; Rash et al. 2016). Primary cultured cortical neurons have been widely used to study neuronal function *in vitro* and to explore the molecular mechanism of neurite outgrowth in the developing central nervous system (Kamijo et al. 2018; Pallaki et al. 2017) as well as to investigate the developmental neurotoxicity and mechanisms of action of drug candidates and environmental toxicants (Cao et al. 2014a, 2014b; George et al. 2012). In this study, we demonstrated that as cortical neuronal networks developed *in vitro*, SCO frequency and ESA increased in concert with morphometric complexity. The temporal increase in morphological complexity coincides with enhanced functional connectivity across the neuronal network that likely mimic many aspects of the developing brain (Feller 1999; Stafford et al. 2009). Importantly, nanomolar DM was shown to be capable of altering both morphometric and functional parameters.

Pyrethroids metabolites have been detected in urine, breast milk, and blood samples (Morgan et al. 2007; Oulhote and Bouchard 2013; Richardson et al. 2015; Wu et al. 2013). Recent epidemiological evidence indicates that environmental exposures to pyrethroid are associated with increased risks of delayed

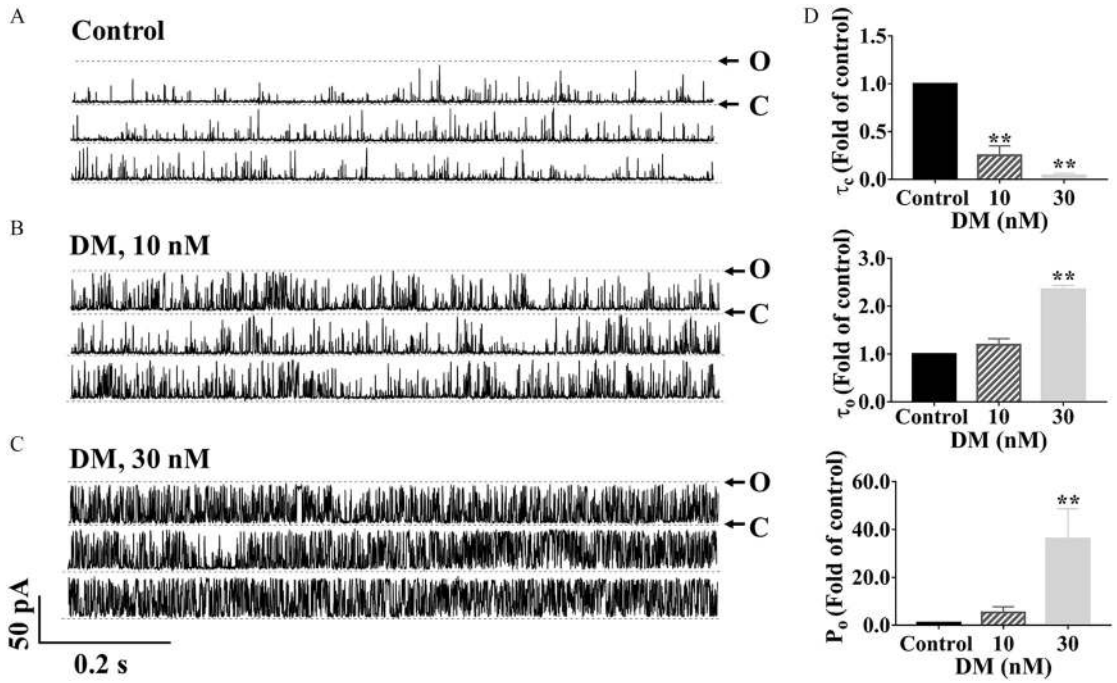

Figure 7. Influence of nanomolar DM on the gating kinetics of RyR1 channels. (A–C) Representative traces of RyR1 activity in single-channel level in the (A) absence, and (B) presence of 10 nM and (C) 30 nM, respectively. (D) Analysis of the gating parameters of mean closed time (τ_c) (top), mean open time (τ_o) (middle), and open probability (P_o) (bottom). Each data point represents the mean ± standard error of the mean (SEM) from three independent channels. Statistical significance between groups was calculated by one-way analysis of variance (ANOVA) followed by post hoc Bonferroni comparison. Note: C, closed state of the channel; DM, deltamethrin; O, open state of the RyR1 channel; P_o, open probability; RyRs, ryanodine receptors; τ_o, mean open time; τ_c, mean closed time. $^{**}p < 0.01$, DM vs. control.

neuronal development (Gunier et al. 2017; Shelton et al. 2014; Xue et al. 2013). Previous results from animal models also indicated that perinatal exposure *in vivo* to low doses of pyrethroid altered the function of central nervous system later in life. For example, prenatal exposure of mice to low doses (0.3 mg/kg and 1 mg/kg every 3 d) of DM resulted in ADHD-like behavior, which was presumably mediated via altered dopaminergic signaling pathways (Richardson et al. 2015). The concentration of DM in brain tissue could reach ~16 ng/g (30 nM) after a single oral dose of 0.5 mg/kg DM in postnatal day 15 and 21 rats (Mortuza et al. 2018). In addition, postnatal exposure to a low dose of cypermethrin (1.5 mg/kg) enhanced the susceptibility of rats to dopaminergic neurodegeneration if rechallenged during adulthood (Singh et al. 2012). Consistent with these findings, prenatal mice receiving low doses (5 mg/kg) of cypermethrin exposure were recently shown to develop abnormal social and adaptive responses that were correlated with changes in brain transcriptional profiles (Laugeray et al. 2017). Additional evidence from zebrafish also indicated the potential of both Type I and Type II pyrethroids to affect neuronal developmental (Bertotto et al. 2018; Frank et al. 2018; Han et al. 2017; Jin et al. 2009; Xu et al. 2018). Here we demonstrated that cortical neurons exposed subchronically to DM (<1 μM) for 6 d displayed concentration-dependent decreases in SCO frequency. Similarly, cortical neurons receiving subchronic DM (10 and 30 nM) exposure for 4 d after plating displayed concentration-dependent inhibition of electrical spike frequency and burst frequency. To our knowledge, these results provide the first evidence that nanomolar concentrations of DM that are relevant to environmental exposures (Morgan et al. 2007; Oulhote and Bouchard 2013; Richardson et al. 2015; Wu et al. 2013) were capable of altering neuronal network activity *in vitro*.

Suppression of electric discharges by DM seemed to wane with longer exposures to (7 vs. 10 vs. 13 d), despite the continuous presence of this pyrethroid. The inhibition of SCO frequency at 6 DIV was slightly more effective than at 8 DIV; however, the level of suppression achieved continued to wane as the neurons developed *in vitro* further. Similarly, although DM displayed similar potency on suppression of SCO amplitude throughout the development stages investigated here, its inhibitory efficacy on SCO amplitude was greater when introduced at earlier stages of development, and this response waned gradually in the neuronal network at more advanced stages of development *in vitro*. Collectively, based on *in vitro* studies, these data suggest that cortical neuronal networks were more sensitive to DM when exposed at early stages of development. There is mounting evidence that pyrethroid neurotoxicity is age dependent and that there are critical windows of susceptibility (Shafer et al. 2005). Neonatal rats were shown to be 16-fold more susceptible than adults to the acute toxicity of DM (Sheets et al. 1994). Similarly, cypermethrin and permethrin were reported to be 17- and sixfold more toxic to neonatal day 8 rats compared with adults (Cantalamessa 1993). The age sensitivity difference can be partially explained by the lower metabolic detoxifying capabilities in rats during the neonatal period (Sheets et al. 1994), consistent with recent toxicokinetic data in which the brain concentration of DM at postnatal day 15 was only ~twofold of that on adult rats (Mortuza et al. 2018). Evidence for age-dependent susceptibility to pyrethroids was also indicated by subchronic and chronic exposure studies in rodent and zebrafish models. Prenatal mice receiving low doses (5 mg/kg) of cypermethrin exposure developed abnormal motor activity and social and adaptive responses (Laugeray et al. 2017), while adults were much less sensitive (Singh et al. 2012). In zebrafish embryos and juveniles, bifenthrin exposure produced opposite effect on dopamine metabolism (Bertotto et al. 2018).

Activity-dependent calcium signaling has been shown to regulate dendritic growth and branching (Konur and Ghosh 2005). An optimal window for $[Ca^{2+}]_i$ is required for activity-dependent

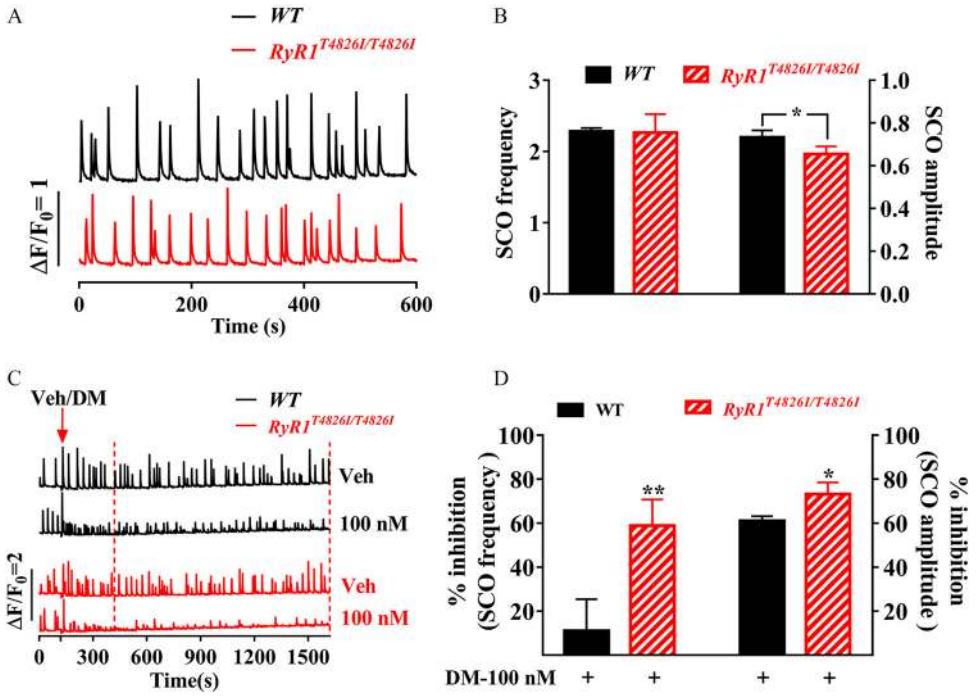

Figure 8. Impacts of RyR1$^{T4826I/T4826I}$ mutation on DM-induced SCO alternation. (A) Representative traces of SCOs in cortical neuronal cultures from WT mice (top trace) and mice carrying RyR1$^{T4826I/T4826I}$ gain-of-function mutation (bottom trace) recorded at 7 DIV. (B) Quantification of the SCO frequency and amplitude in WT and RyR1$^{T4828I/T4826I}$ neurons. (C) Representative SCO traces in the absence and presence of DM (100 nM) in WT (upper two traces) and RyR1$^{T4828I/T4826I}$ neurons (lower two traces). Arrowhead indicates the addition of Veh (0.1% DMSO) or DM (100 nM). The data from dashed line window were used to analyze the inhibitions. (D) Quantification of DM inhibitions on the SCO frequency and amplitude in WT and RyR1$^{T4828I/T4826I}$ neurons. DM-induced response (% inhibition) was analyzed by normalizing to respective vehicle control (0.1% DMSO) of each genotype. The mean values of SCO frequency and amplitude of each plate were used as analysis unit. Each data points represents the mean ± standard error of the mean (SEM) from four independent sister cultures. A *t*-test was used to compare the statistical significance of SCO frequency and amplitude between WT and RyR1$^{T4826I/T4826I}$ neurons as well as the SCO response of DM between two genotypes. Note: DM, deltamethrin; DMSO, dimethylsulfoxide; RyRs, ryanodine receptors; SCO, synchronous Ca^{2+} oscillations; Veh, vehicle; WT, wild type. $*p < 0.05$; $**p < 0.01$, WT neurons vs. RyR1$^{T4828I/T4826I}$ neurons.

neurite extension and branching. Small to moderate amplification of Ca^{2+} signaling stimulates dendritic growth, whereas excessive Ca^{2+} alteration may stall dendritic growth (Gomez and Spitzer 2000; Hui et al. 2007). Our data demonstrated that DM-modulated Ca^{2+} signaling was sufficient to alter axonal growth and neuronal complexity. DM exposure produced nonmonotonic response on the stimulation of axonal growth and neuronal complexity, with peak response occurring at 100 and 300 nM, respectively. The concentration-dependent profiles of DM-stimulated axon growth and neuron complexity were therefore consistent with activity-dependent dendritic growth (Gomez and Spitzer 2000; Hui et al. 2007). It was reported that DM at 1 μM increased neurite outgrowth in rat cortical neurons through endogenous BDNF/tropomyosin receptor kinase B pathways (Ihara et al. 2017). However, in the current study, we demonstrated that DM (1 μM) affected neither axon growth nor dendritic branching. One of the main factors that may contribute to this discrepancy could be the use of neurons at different stages of development, especially considering the distinct susceptibility to DM exposure in distinct developmental stages discussed above. Another factor that may also contribute to the discrepancy could be the exposure duration. We treated neurons for 48 h and 6 d commencing 3 h after plating for axon growth and dendritic complexity measurements, respectively, while in the previous study, neurons were exposed at 7 DIV for 3, 6, 12, and 24 h, respectively (Ihara et al. 2017).

RyRs are Ca^{2+} channels that regulate Ca^{2+} release from the sarco/endoplasmic reticulum (Pessah et al. 2010). All three subtypes of RyRs were reported to be expressed in the central nervous system (Feng et al. 2017; Galeotti et al. 2008; Giannini et al. 1995; Kurokawa et al. 2011; Meissner 2002). We demonstrated that alteration of RyR1 function was sufficient to affect functional outcomes of *in vitro* neuronal networks. Primary cultured cortical neuronal network from the mouse pups carrying RyR1$^{T4826I/T4826I}$ gain-of-function mutation exhibited significantly lower SCO amplitude and much longer axons. This was consistent with the demonstration that RyRs were responsible for producing temporally and spatially defined Ca^{2+} signals important for neuronal growth and plasticity (Ohashi et al. 2014; Wayman et al. 2012a; Wilson et al. 2016). DM has been reported to alter a variety of channel functions (Clark and Symington 2012; Soderlund 2012). Using Golgi staining of brain section, Keil and coworkers (Keil et al. 2019) recently reported that CA1 hippocampal pyramidal neurons of young male RyR1$^{T4826I/T4826I}$ mice exhibit significantly increased dendritic arborization compared with WT, whereas genotype differences could be detected within the somatosensory cortex of both sexes. Importantly, such morphometric changes in complexity were correlated with behavioral performance in the three-chambered social approach test (Keil et al. 2019).

We demonstrated that DM altered RyR1 gating kinetics at levels as low as 10 nM, providing the evidence that RyR1 was a direct sensitive target of DM. It should be mentioned that >3 μM DM was required to elicit changes in specific [^{3}H]Ry binding to RyR1, RyR2, and a mixture of three types of RyRs prepared from cortex. This apparent discrepancy may be due to an underestimate of the true potency because of the high lipid content in the microsomal preparations used in these assays and the high lipophilicity of DM. This phenomenon was also observed for lipophilic polychlorinated biphenyls (PCBs), such as PCB-202 and PCB-95 (Holland et al.

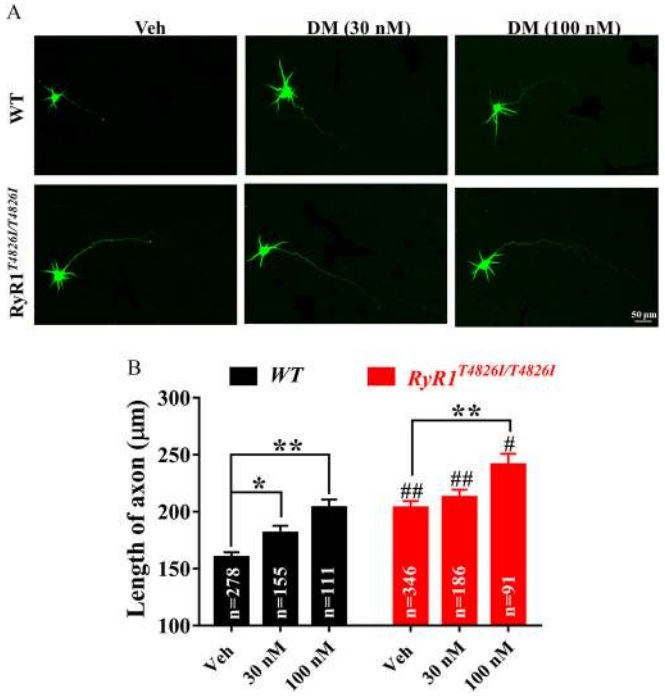

Figure 9. Impacts of RyR1$^{T4826I/T4826I}$ mutation on DM-induced axonal outgrowth. (A) Representative images of WT and RyR1$^{T4826I/T4826I}$ mutation neurons exposed to Veh (0.1% DMSO) and DM (30 nM and 100 nM) commencing 3 h after plating and immunostained with MAP-2B antibody at 2 DIV. (B) Quantification of the axon length after DM exposure in WT and RyR1$^{T4826I/T4826I}$ mutation neurons. The total number of neurons tested was inserted in the bar graph, and axonal length of each neuron was used as analysis unit. Each data point represents the mean ± standard error of the mean (SEM) from two independent sister cultures, each with three wells. Statistical significance between WT and RyR1$^{T4826I/T4826I}$ neurons was performed using two-way analysis of variance (ANOVA) followed by post hoc Bonferroni comparison. Note: DM, deltamethrin; DMSO, dimethylsulfoxide; RyRs, ryanodine receptors; Veh, vehicle; WT, wild type. $^{*}p < 0.05$; $^{**}p < 0.01$, DM vs. Veh; $^{\#}p < 0.05$; $^{\#\#}p < 0.01$, RyR1$^{T4826I/T4826I}$ vs. WT at same treatment condition. Bar = 50 μm.

2017; Sethi et al. 2019; Wayman et al. 2012a, 2012b). Additional evidence of involvement of RyR1 as a molecular target of DM-induced changes in functional neuronal network came from the results of experiments with neural networks expressing the gain-of-function mutation RyR1$^{T4826I/T4826I}$, which showed additional effect in response to DM exposure. Likewise, we could not rule out other potential molecular targets such as $Ca_v2.2$ that were reported to be highly sensitive to DM exposure (Clark and Symington 2008; Symington and Clark 2005). We previously demonstrated that bifenthrin altered the SCO patterns at nanomolar concentrations, apparently without direct effect on the gating kinetics of RyR1 (Cao et al. 2014b). More recently, however, exposure of zebrafish to bifenthrin 1, 3, and 5 d postfertilization was shown to alter transcriptional regulation of RyRs and elements in the mechanistic target of rapamycin (mTOR) signaling pathway (Frank et al. 2018). Therefore, it appears that RyRs may be involved either directly or indirectly in neurotoxicity of both Type I (bifenthrin) and Type II (DM) pyrethroids.

In summary, we demonstrated that DM at nanomolar concentrations altered the cortical neuronal network excitability, axonal growth, and dendritic arborization of neuronal cells *in vitro*. We also identified that neuronal networks exposed early in their *in vitro* developmental stages were more sensitive to low nanomolar DM exposure than later stages, consistent with recent reports from *in vivo* vertebrate models of exposure. Importantly, we provided direct evidence that low nanomolar DM directly engaged RyR and altered channel function, identifying a highly sensitive target that may be generalizable to other Type II pyrethroids.

Acknowledgments

This work was supported by National Natural Science Foundation of China (21777192, 81473539); "Double First-Class" project of China Pharmaceutical University (CPU2018GY18), China Scholarship Council (201507060027), U.S. National Institute of Environmental Health Sciences (R01 ES014901, P01 ES011269, and P42 ES04699), and the U.S. Environmental Protection Agency [STAR R829388 and R833292].

References

Amweg EL, Weston DP, Ureda NM. 2005. Use and toxicity of pyrethroid pesticides in the Central Valley, California, USA. Environ Toxicol Chem 24(4):966–972, PMID: 15839572, https://doi.org/10.1897/04-146R1.1.

Barrientos GC, Feng W, Truong K, Matthaei KI, Yang T, Allen PD, et al. 2012. Gene dose influences cellular and calcium channel dysregulation in heterozygous and homozygous T4826I-RyR1 malignant hyperthermia-susceptible muscle. J Biol Chem 287(4):2863–2876, PMID: 22139840, https://doi.org/10.1074/jbc.M111.307926.

Berridge MJ. 2014. Calcium regulation of neural rhythms, memory and Alzheimer's disease. J Physiol 592(2):281–293, PMID: 23753528, https://doi.org/10.1113/jphysiol.2013.257527.

Bertotto LB, Richards J, Gan J, Volz DC, Schlenk D. 2018. Effects of bifenthrin exposure on the estrogenic and dopaminergic pathways in zebrafish embryos and juveniles. Environ Toxicol Chem 37(1):236–246, PMID: 28815728, https://doi.org/10.1002/etc.3951.

Brooks SP, Storey KB. 1992. Bound and determined: a computer program for making buffers of defined ion concentrations. Anal Biochem 201(1):119–126, PMID: 1621949, https://doi.org/10.1016/0003-2697(92)90183-8.

Cáceres A, Banker GA, Binder L. 1986. Immunocytochemical localization of tubulin and microtubule-associated protein 2 during the development of hippocampal neurons in culture. J Neurosci 6(3):714–722, PMID: 3514816, https://doi.org/10.1523/JNEUROSCI.06-03-00714.1986.

Cantalamessa F. 1993. Acute toxicity of two pyrethroids, permethrin, and cypermethrin in neonatal and adult rats. Arch Toxicol 67(7):510–513, PMID: 8240001, https://doi.org/10.1007/BF01969923.

Cao Z, Cui Y, Busse E, Mehrotra S, Rainier JD, Murray TF. 2014a. Gambierol inhibition of voltage-gated potassium channels augments spontaneous Ca^{2+} oscillations in cerebrocortical neurons. J Pharmacol Exp Ther 350(3):615–623, PMID: 24957609, https://doi.org/10.1124/jpet.114.215319.

Cao Z, Cui Y, Nguyen HM, Jenkins DP, Wulff H, Pessah IN. 2014b. Nanomolar bifenthrin alters synchronous Ca^{2+} oscillations and cortical neuron development independent of sodium channel activity. Mol Pharmacol 85(4):630–639, PMID: 24482397, https://doi.org/10.1124/mol.113.090076.

Cao Z, Hammock BD, McCoy M, Rogawski MA, Lein PJ, Pessah IN. 2012a. Tetramethylenedisulfotetramine alters Ca^{2+} dynamics in cultured hippocampal neurons: mitigation by NMDA receptor blockade and $GABA_A$ receptor-positive modulation. Toxicol Sci 130(2):362–372, PMID: 22889812, https://doi.org/10.1093/toxsci/kfs244.

Cao Z, Hulsizer S, Tassone F, Tang HT, Hagerman RJ, Rogawski MA, et al. 2012b. Clustered burst firing in FMR1 premutation hippocampal neurons: amelioration with allopregnanolone. Hum Mol Genet 21(13):2923–2935, PMID: 22466801, https://doi.org/10.1093/hmg/dds118.

Cao Z, Shafer TJ, Crofton KM, Gennings C, Murray TF. 2011a. Additivity of pyrethroid actions on sodium influx in cerebrocortical neurons in primary culture. Environ Health Perspect 119(9):1239–1246, PMID: 21665567, https://doi.org/10.1289/ehp.1003394.

Cao Z, Shafer TJ, Murray TF. 2011b. Mechanisms of pyrethroid insecticide-induced stimulation of calcium influx in neocortical neurons. J Pharmacol Exp Ther 336(1):197–205, PMID: 20881019, https://doi.org/10.1124/jpet.110.171850.

Cao Z, Xu J, Hulsizer S, Cui Y, Dong Y, Pessah IN. 2017. Influence of tetramethylenedisulfotetramine on synchronous calcium oscillations at distinct developmental stages of hippocampal neuronal cultures. Neurotoxicology 58:11–22, PMID: 27984050, https://doi.org/10.1016/j.neuro.2016.10.015.

Cao Z, Zou X, Cui Y, Hulsizer S, Lein PJ, Wulff H, et al. 2015. Rapid throughput analysis demonstrates that chemicals with distinct seizurogenic mechanisms differentially alter Ca^{2+} dynamics in networks formed by hippocampal neurons in culture. Mol Pharmacol 87(4):595–605, PMID: 25583085, https://doi.org/10.1124/mol.114.096701.

Casida JE, Quistad GB. 1998. Golden age of insecticide research: past, present, or future? Annu Rev Entomol 43(1):1–16, PMID: 9444749, https://doi.org/10.1146/annurev.ento.43.1.1.

Castellanos A, Andres A, Bernal L, Callejo G, Comes N, Gual A, et al. 2018. Pyrethroids inhibit K2P channels and activate sensory neurons: basis of insecticide-induced paraesthesias. Pain 159(1):92–105, PMID: 28937579, https://doi.org/10.1097/j.pain.0000000000001068.

Chen H, Streifel KM, Singh V, Yang DR, Mangini L, Wulff H, et al. 2017. From the cover: BDE-47 and BDE-49 inhibit axonal growth in primary rat hippocampal neuron-glia co-cultures via ryanodine receptor-dependent mechanisms. Toxicol Sci 156:375–386, PMID: 28003438, https://doi.org/10.1093/toxsci/kfw259.

Clark JM, Symington SB. 2008. Neurotoxic implications of the agonistic action of CS-syndrome pyrethroids on the N-type $Ca_v2.2$ calcium channel. Pest Manag Sci 64(6):628–638, PMID: 18383452, https://doi.org/10.1002/ps.1573.

Clark JM, Symington SB. 2012. Advances in the mode of action of pyrethroids. Top Curr Chem 314:49–72, PMID: 22025067, https://doi.org/10.1007/128_2011_268.

Corcellas C, Feo ML, Torres JP, Malm O, Ocampo-Duque W, Eljarrat E, et al. 2012. Pyrethroids in human breast milk: occurrence and nursing daily intake estimation. Environ Int 47:17–22, PMID: 22717642, https://doi.org/10.1016/j.envint.2012.05.007.

Cotterill E, Hall D, Wallace K, Mundy WR, Eglen SJ, Shafer TJ. 2016. Characterization of early cortical neural network development in multiwell microelectrode array plates. J Biomol Screen 21(5):510–519, PMID: 27028607, https://doi.org/10.1177/1087057116640520.

Dereumeaux C, Saoudi A, Goria S, Wagner V, De Crouy-Chanel P, Pecheux M, et al. 2018. Urinary levels of pyrethroid pesticides and determinants in pregnant French women from the Elfe cohort. Environ Int 119:89–99, PMID: 29944988, https://doi.org/10.1016/j.envint.2018.04.042.

Dolmetsch RE, Xu K, Lewis RS. 1998. Calcium oscillations increase the efficiency and specificity of gene expression. Nature 392(6679):933–936, PMID: 9582075, https://doi.org/10.1038/31960.

Dotti CG, Sullivan CA, Banker GA. 1988. The establishment of polarity by hippocampal neurons in culture. J Neurosci 8(4):1454–1468, PMID: 3282038, https://doi.org/10.1523/JNEUROSCI.08-04-01454.1988.

Dravid SM, Murray TF. 2004. Spontaneous synchronized calcium oscillations in neocortical neurons in the presence of physiological [Mg^{2+}]: involvement of AMPA/kainate and metabotropic glutamate receptors. Brain Res 1006(1):8–17, PMID: 15047019, https://doi.org/10.1016/j.brainres.2004.01.059.

Feller MB. 1999. Spontaneous correlated activity in developing neural circuits. Neuron 22(4):653–656, PMID: 10230785, https://doi.org/10.1016/S0896-6273(00)80724-2.

Feng W, Zheng J, Robin G, Dong Y, Ichikawa M, Inoue Y, et al. 2017. Enantioselectivity of 2,2',3,5',6-pentachlorobiphenyl (PCB 95) atropisomers toward ryanodine receptors (RyRs) and their influences on hippocampal neuronal networks. Environ Sci Technol 51(24):14406–14416, PMID: 29131945, https://doi.org/10.1021/acs.est.7b04446.

Ferreira TA, Blackman AV, Oyrer J, Jayabal S, Chung AJ, Watt AJ, et al. 2014. Neuronal morphometry directly from bitmap images. Nat Methods 11(10):982–984, PMID: 25264773, https://doi.org/10.1038/nmeth.3125.

Field LM, Emyr Davies TG, O'Reilly AO, Williamson MS, Wallace BA. 2017. Voltage-gated sodium channels as targets for pyrethroid insecticides. Eur Biophys J 46(7):675–679, PMID: 28070661, https://doi.org/10.1007/s00249-016-1195-1.

Forshaw PJ, Lister T, Ray DE. 1993. Inhibition of a neuronal voltage-dependent chloride channel by the type II pyrethroid, deltamethrin. Neuropharmacology 32(2):105–111, PMID: 8383811, https://doi.org/10.1016/0028-3908(93)90089-L.

Frank DF, Miller GW, Harvey DJ, Brander SM, Geist J, Connon RE, et al. 2018. Bifenthrin causes transcriptomic alterations in mTOR and ryanodine receptor-dependent signaling and delayed hyperactivity in developing zebrafish (Danio rerio). Aquat Toxicol 200:50–61, PMID: 29727771, https://doi.org/10.1016/j.aquatox.2018.04.003.

Frega M, Pasquale V, Tedesco M, Marcoli M, Contestabile A, Nanni M, et al. 2012. Cortical cultures coupled to micro-electrode arrays: a novel approach to perform in vitro excitotoxicity testing. Neurotoxicol Teratol 34(1):116–127, PMID: 21856414, https://doi.org/10.1016/j.ntt.2011.08.001.

Galeotti N, Quattrone A, Vivoli E, Norcini M, Bartolini A, Ghelardini C. 2008. Different involvement of type 1, 2, and 3 ryanodine receptors in memory processes. Learn Mem 15(5):315–323, PMID: 18441289, https://doi.org/10.1101/lm.929008.

Gan JJ. 2008. *Synthetic Pyrethroids: Occurrence and Behavior in Aquatic Environments*. Washington, DC:American Chemical Society.

George J, Baden DG, Gerwick WH, Murray TF. 2012. Bidirectional influence of sodium channel activation on NMDA receptor-dependent cerebrocortical neuron structural plasticity. Proc Natl Acad Sci U S A 109(48):19840–19845, PMID: 23150561, https://doi.org/10.1073/pnas.1212584109.

Giannini G, Conti A, Mammarella S, Scrobogna M, Sorrentino V. 1995. The ryanodine receptor/calcium channel genes are widely and differentially expressed in murine brain and peripheral tissues. J Cell Biol 128(5):893–904, PMID: 7876312, https://doi.org/10.1083/jcb.128.5.893.

Gomez TM, Spitzer NC. 2000. Regulation of growth cone behavior by calcium: new dynamics to earlier perspectives. J Neurobiol 44(2):174–183, PMID: 10934320, https://doi.org/10.1002/1097-4695(200008)44:2<174::AID-NEU7>3.0.CO;2-R.

Gunier RB, Bradman A, Harley KG, Kogut K, Eskenazi B. 2017. Prenatal residential proximity to agricultural pesticide use and IQ in 7-year-old children. Environ Health Perspect 125(5):057002, PMID: 28557711, https://doi.org/10.1289/EHP504.

Han J, Ji C, Guo Y, Yan R, Hong T, Dou Y, et al. 2017. Mechanisms underlying melatonin-mediated prevention of fenvalerate-induced behavioral and oxidative toxicity in zebrafish. J Toxicol Environ Health A 80(23-24):1331–1341, PMID: 29144200, https://doi.org/10.1080/15287394.2017.1384167.

Harrill JA, Robinette BL, Mundy WR. 2011. Use of high content image analysis to detect chemical-induced changes in synaptogenesis in vitro. Toxicol In Vitro 25(1):368–387, PMID: 20969947, https://doi.org/10.1016/j.tiv.2010.10.011.

Holland EB, Feng W, Zheng J, Dong Y, Li X, Lehmler HJ, et al. 2017. An extended structure–activity relationship of nondioxin-like PCBs evaluates and supports modeling predictions and identifies picomolar potency of PCB 202 towards ryanodine receptors. Toxicol Sci 155(1):170–181, PMID: 27655348, https://doi.org/10.1093/toxsci/kfw189.

Hui K, Fei GH, Saab BJ, Su J, Roder JC, Feng ZP. 2007. Neuronal calcium sensor-1 modulation of optimal calcium level for neurite outgrowth. Development 134(24):4479–4489, PMID: 18039973, https://doi.org/10.1242/dev.008979.

Ihara D, Fukuchi M, Honma D, Takasaki I, Ishikawa M, Tabuchi A, et al. 2012. Deltamethrin, a type ii pyrethroid insecticide, has neurotrophic effects on neurons with continuous activation of the Bdnf promoter. Neuropharmacology 62(2):1091–1098, PMID: 22079160, https://doi.org/10.1016/j.neuropharm.2011.10.023.

Ihara D, Fukuchi M, Honma D, Takasaki I, Tabuchi A, Tsuda M. 2011. Deltamethrin, a type II pyrethroid insecticide, induces marked BDNF mRNA expression and morphological changes by maintaining the elevated concentration of calcium in cultured cortical neurons. Neuroscience Research 71:e121, PMID: 22079160, https://doi.org/10.1016/j.neures.2011.07.515.

Ihara D, Fukuchi M, Katakai M, Shinoda Y, Katoh-Semba R, Furuichi T, et al. 2017. Deltamethrin increases neurite outgrowth in cortical neurons through endogenous BDNF/TrkB pathways. Cell Struct Funct 42(2):141–148, PMID: 28943602, https://doi.org/10.1247/csf.17015.

Jin M, Zhang X, Wang L, Huang C, Zhang Y, Zhao M. 2009. Developmental toxicity of bifenthrin in embryo-larval stages of zebrafish. Aquat Toxicol 95(4):347–354, PMID: 19880199, https://doi.org/10.1016/j.aquatox.2009.10.003.

Kamijo S, Ishii Y, Horigane SI, Suzuki K, Ohkura M, Nakai J, et al. 2018. A critical neurodevelopmental role for L-type voltage-gated calcium channels in neurite extension and radial migration. J Neurosci 38(24):5551–5566, PMID: 29773754, https://doi.org/10.1523/JNEUROSCI.2357-17.2018.

Kaplan A, Morquette B, Kroner A, Leong S, Madwar C, Sanz R, et al. 2017. Small-molecule stabilization of 14-3-3 protein-protein interactions stimulates axon regeneration. Neuron 93(5):1082–1093, PMID: 28279353, https://doi.org/10.1016/j.neuron.2017.02.018.

Keil KP, Sethi S, Wilson MD, Silverman JL, Pessah IN, Lein PJ. 2019. Genetic mutations in Ca^{2+} signaling alter dendrite morphology and social approach in juvenile mice. Genes Brain Behav 18(1):e12526, PMID: 30311737, https://doi.org/10.1111/gbb.12526.

Konur S, Ghosh A. 2005. Calcium signaling and the control of dendritic development. Neuron 46(3):401–405, PMID: 15882639, https://doi.org/10.1016/j.neuron.2005.04.022.

Kurokawa K, Mizuno K, Kiyokage E, Shibasaki M, Toida K, Ohkuma S. 2011. Dopamine D1 receptor signaling system regulates ryanodine receptor expression after intermittent exposure to methamphetamine in primary cultures of midbrain and cerebral cortical neurons. J Neurochem 118(5):773–783, PMID: 21707617, https://doi.org/10.1111/j.1471-4159.2011.07366.x.

Lanner JT, Georgiou DK, Joshi AD, Hamilton SL. 2010. Ryanodine receptors: structure, expression, molecular details, and function in calcium release. Cold Spring Harb Perspect Biol 2(11):a003996, PMID: 20961976, https://doi.org/10.1101/cshperspect.a003996.

Laugeray A, Herzine A, Perche O, Richard O, Montecot-Dubourg C, Menuet A, et al. 2017. In utero and lactational exposure to low-doses of the pyrethroid insecticide cypermethrin leads to neurodevelopmental defects in male mice-an ethological and transcriptomic study. PLoS One 12(10):e0184475, PMID: 29020013, https://doi.org/10.1371/journal.pone.0184475.

Li F, Ma H, Liu J. 2018. Pyrethroid insecticide cypermethrin modulates gonadotropin synthesis via calcium homeostasis and ERK1/2 signaling in LβT2 mouse pituitary cells. Toxicol Sci 162(1):43–52, PMID: 29149324, https://doi.org/10.1093/toxsci/kfx248.

Meijer M, Dingemans MM, van den Berg M, Westerink RH. 2014. Inhibition of voltage-gated calcium channels as common mode of action for (mixtures of) distinct classes of insecticides. Toxicol Sci 141(1):103–111, PMID: 24913802, https://doi.org/10.1093/toxsci/kfu110.

Meijering E, Jacob M, Sarria JC, Steiner P, Hirling H, Unser M. 2004. Design and validation of a tool for neurite tracing and analysis in fluorescence microscopy images. Cytometry A 58(2):167–176, PMID: 15057970, https://doi.org/10.1002/cyto.a.20022.

Meissner G. 2002. Regulation of mammalian ryanodine receptors. Front Biosci 7(4): d2072–2080, PMID: 12438018, https://doi.org/10.2741/A899.
Morgan MK, Sheldon LS, Croghan CW, Jones PA, Chuang JC, Wilson NK. 2007. An observational study of 127 preschool children at their homes and daycare centers in Ohio: environmental pathways to cis- and trans-permethrin exposure. Environ Res 104(2):266–274, PMID: 17258193, https://doi.org/10.1016/j.envres.2006.11.011.
Morisseau C, Merzlikin O, Lin A, He G, Feng W, Padilla I, et al. 2009. Toxicology in the fast lane: application of high-throughput bioassays to detect modulation of key enzymes and receptors. Environ Health Perspect 117(12):1867–1872, PMID: 20049205, https://doi.org/10.1289/ehp.0900834.
Mortuza T, Chen C, White CA, Cummings BS, Muralidhara S, Gullick D, et al. 2018. Toxicokinetics of deltamethrin: dosage dependency, vehicle effects, and low-dose age-equivalent dosimetry in rats. Toxicol Sci 162(1):327–336, PMID: 29165640, https://doi.org/10.1093/toxsci/kfx260.
Mukai J, Tamura M, Fénelon K, Rosen AM, Spellman TJ, Kang R, et al. 2015. Molecular substrates of altered axonal growth and brain connectivity in a mouse model of schizophrenia. Neuron 86(3):680–695, PMID: 25913858, https://doi.org/10.1016/j.neuron.2015.04.003.
Narahashi T. 1985. Nerve membrane ionic channels as the primary target of pyrethroids. Neurotoxicology 6(2):3–22, PMID: 2410830.
Ohashi R, Sakata S, Naito A, Hirashima N, Tanaka M. 2014. Dendritic differentiation of cerebellar Purkinje cells is promoted by ryanodine receptors expressed by Purkinje and granule cells. Dev Neurobiol 74(4):467–480, PMID: 24123915, https://doi.org/10.1002/dneu.22139.
Oulhote Y, Bouchard MF. 2013. Urinary metabolites of organophosphate and pyrethroid pesticides and behavioral problems in Canadian children. Environ Health Perspect 121(11-12):1378–1384, PMID: 24149046, https://doi.org/10.1289/ehp.1306667.
Pacico N, Mingorance-Le Meur A. 2014. New in vitro phenotypic assay for epilepsy: fluorescent measurement of synchronized neuronal calcium oscillations. PLoS One 9(1):e84755, PMID: 24416277, https://doi.org/10.1371/journal.pone.0084755.
Pallaki P, Georganta EM, Serafimidis I, Papakonstantinou MP, Papanikolaou V, Koutloglou S, et al. 2017. A novel regulatory role of RGS4 in STAT5B activation, neurite outgrowth and neuronal differentiation. Neuropharmacology 117:408–421, PMID: 28219718, https://doi.org/10.1016/j.neuropharm.2017.02.012.
Pessah IN, Cherednichenko G, Lein PJ. 2010. Minding the calcium store: ryanodine receptor activation as a convergent mechanism of PCB toxicity. Pharmacol Therapeut 125(2):260–285, PMID: 19931307, https://doi.org/10.1016/j.pharmthera.2009.10.009.
Pessah IN, Waterhouse AL, Casida JE. 1985. The calcium-ryanodine receptor complex of skeletal and cardiac muscle. Biochem Biophys Res Commun 128(1):449–456, PMID: 3985981, https://doi.org/10.1016/0006-291X(85)91699-7.
Qi X, Zheng M, Wu C, Wang G, Feng C, Zhou Z. 2012. Urinary pyrethroid metabolites among pregnant women in an agricultural area of the province of Jiangsu, China. Int J Hyg Environ Health 215(5):487–495, PMID: 22218106, https://doi.org/10.1016/j.ijheh.2011.12.003.
Rash BG, Ackman JB, Rakic P. 2016. Bidirectional radial Ca^{2+} activity regulates neurogenesis and migration during early cortical column formation. Sci Adv 2(2):e1501733, PMID: 26933693, https://doi.org/10.1126/sciadv.1501733.
Richardson JR, Taylor MM, Shalat SL, Guillot TS 3rd, Caudle WM, Hossain MM, et al. 2015. Developmental pesticide exposure reproduces features of attention deficit hyperactivity disorder. FASEB J 29(5):1960–1972, PMID: 25630971, https://doi.org/10.1096/fj.14-260901.
Romero A, Ramos E, Castellano V, Martinez MA, Ares I, Martinez M, et al. 2012. Cytotoxicity induced by deltamethrin and its metabolites in SH-SY5Y cells can be differentially prevented by selected antioxidants. Toxicol In Vitro 26(6):823–830, PMID: 22634057, https://doi.org/10.1016/j.tiv.2012.05.004.
Saillenfait AM, Ndiaye D, Sabaté JP. 2015. Pyrethroids: exposure and health effects–an update. Int J Hyg Environ Health 218(3):281–292, PMID: 25648288, https://doi.org/10.1016/j.ijheh.2015.01.002.
Saito A, Seiler S, Chu A, Fleischer S. 1984. Preparation and morphology of sarcoplasmic reticulum terminal cisternae from rabbit skeletal muscle. J Cell Biol 99(3):875–885, PMID: 6147356, https://doi.org/10.1083/jcb.99.3.875.
Sethi S, Morgan R, Feng W, Lin Y, Li X, Luna C, et al. 2019. Comparative analyses of the 12 most abundant PCB congeners detected in human maternal serum for activity at the thyroid hormone receptor and ryanodine receptor. Environ Sci Technol 53(7):3948–3958, PMID: 30821444, https://doi.org/10.1021/acs.est.9b00535.
Shafer TJ, Meyer DA, Crofton KM. 2005. Developmental neurotoxicity of pyrethroid insecticides: critical review and future research needs. Environ Health Perspect 113(2):123–136, PMID: 15687048, https://doi.org/10.1289/ehp.7254.
Sharma A, Gill JP, Bedi JS, Pooni PA. 2014. Monitoring of pesticide residues in human breast milk from Punjab, India and its correlation with health associated parameters. Bull Environ Contam Toxicol 93(4):465–471, PMID: 25011502, https://doi.org/10.1007/s00128-014-1326-2.
Sheets LP, Doherty JD, Law MW, Reiter LW, Crofton KM. 1994. Age-dependent differences in the susceptibility of rats to deltamethrin. Toxicol Appl Pharmacol 126(1):186–190, PMID: 8184428, https://doi.org/10.1006/taap.1994.1106.
Shelton JF, Geraghty EM, Tancredi DJ, Delwiche LD, Schmidt RJ, Ritz B, et al. 2014. Neurodevelopmental disorders and prenatal residential proximity to agricultural pesticides: the CHARGE study. Environ Health Perspect 122(10):1103–1109, PMID: 24954055, https://doi.org/10.1289/ehp.1307044.
Siebler M, Koller H, Stichel CC, Muller HW, Freund HJ. 1993. Spontaneous activity and recurrent inhibition in cultured hippocampal networks. Synapse 14(3):206–213, PMID: 8211707, https://doi.org/10.1002/syn.890140304.
Singh C, Liu L, Wang JM, Irwin RW, Yao J, Chen S, et al. 2012. Allopregnanolone restores hippocampal-dependent learning and memory and neural progenitor survival in aging 3xTgAD and nonTg mice. Neurobiol Aging 33(8):1493–1506, PMID: 21803451, https://doi.org/10.1016/j.neurobiolaging.2011.06.008.
Smith NA, Kress BT, Lu Y, Chandler-Militello D, Benraiss A, Nedergaard M. 2018. Fluorescent Ca^{2+} indicators directly inhibit the Na,K-ATPase and disrupt cellular functions. Sci Signal 11(515):eaal2039, PMID: 29382785, https://doi.org/10.1126/scisignal.aal2039.
Soderlund DM. 2012. Molecular mechanisms of pyrethroid insecticide neurotoxicity: recent advances. Arch Toxicol 86(2):165–181, PMID: 21710279, https://doi.org/10.1007/s00204-011-0726-x.
Soderlund DM, Clark JM, Sheets LP, Mullin LS, Piccirillo VJ, Sargent D, et al. 2002. Mechanisms of pyrethroid neurotoxicity: implications for cumulative risk assessment. Toxicology 171(1):3–59, PMID: 11812616, https://doi.org/10.1016/S0300-483X(01)00569-8.
Spitzer NC, Olson E, Gu X. 1995. Spontaneous calcium transients regulate neuronal plasticity in developing neurons. J Neurobiol 26(3):316–324, PMID: 7775965, https://doi.org/10.1002/neu.480260304.
Stafford BK, Sher A, Litke AM, Feldheim DA. 2009. Spatial-temporal patterns of retinal waves underlying activity-dependent refinement of retinofugal projections. Neuron 64(2):200–212, PMID: 19874788, https://doi.org/10.1016/j.neuron.2009.09.021.
Symington SB, Clark JM. 2005. Action of deltamethrin on N-type $Ca_v2.2$ voltage-sensitive calcium channels in rat brain. Pestic Biochem Physiol 82(1):1–15, https://doi.org/10.1016/j.pestbp.2004.11.006.
Taylor-Wells J, Brooke BD, Bermudez I, Jones AK. 2015. The neonicotinoid imidacloprid, and the pyrethroid deltamethrin, are antagonists of the insect Rdl GABA receptor. J Neurochem 135(4):705–713, PMID: 26296809, https://doi.org/10.1111/jnc.13290.
Torres-Espin A, Santos D, González-Perez F, del Valle J, Navarro X. 2014. Neurite-J: an image-J plug-in for axonal growth analysis in organotypic cultures. J Neurosci Methods 236:26–39, PMID: 25124852, https://doi.org/10.1016/j.jneumeth.2014.08.005.
Vardi R, Goldental A, Sardi S, Sheinin A, Kanter I. 2016. Simultaneous multi-patch-clamp and extracellular-array recordings: single neuron reflects network activity. Sci Rep 6:36228, PMID: 27824075, https://doi.org/10.1038/srep36228.
Vijverberg HP, van der Zalm JM, van der Bercken J. 1982. Similar mode of action of pyrethroids and ddt on sodium-channel gating in myelinated nerves. Nature 295(5850):601–603, PMID: 6276777.
Wayman GA, Bose DD, Yang D, Lesiak A, Bruun D, Impey S, et al. 2012a. PCB-95 modulates the calcium-dependent signaling pathway responsible for activity-dependent dendritic growth. Environ Health Perspect 120(7):1003–1009, PMID: 22534176, https://doi.org/10.1289/ehp.1104833.
Wayman GA, Impey S, Marks D, Saneyoshi T, Grant WF, Derkach V, et al. 2006. Activity-dependent dendritic arborization mediated by CaM-kinase I activation and enhanced CREB-dependent transcription of Wnt-2. Neuron 50(6):897–909, PMID: 16772171, https://doi.org/10.1016/j.neuron.2006.05.008.
Wayman GA, Yang D, Bose DD, Lesiak A, Ledoux V, Bruun D, et al. 2012b. PCB-95 promotes dendritic growth via ryanodine receptor-dependent mechanisms. Environ Health Perspect 120(7):997–1002, PMID: 22534141, https://doi.org/10.1289/ehp.1104832.
Wilson C, Muñoz-Palma E, Henriquez DR, Palmisano I, Núñez MT, Di Giovanni S, et al. 2016. A feed-forward mechanism involving the NOX complex and RyR-mediated Ca^{2+} release during axonal specification. J Neurosci 36(43):11107–11119, PMID: 27798190, https://doi.org/10.1523/JNEUROSCI.1455-16.2016.
Wolansky MJ, Harrill JA. 2008. Neurobehavioral toxicology of pyrethroid insecticides in adult animals: a critical review. Neurotoxicol Teratol 30(2):55–78, PMID: 18206347, https://doi.org/10.1016/j.ntt.2007.10.005.
Wong PW, Brackney WR, Pessah IN. 1997. Ortho-substituted polychlorinated biphenyls alter microsomal calcium transport by direct interaction with ryanodine receptors of mammalian brain. J Biol Chem 272(24):15145–15153, PMID: 9182535, https://doi.org/10.1074/jbc.272.24.15145.
Wu C, Feng C, Qi X, Wang G, Zheng M, Chang X, et al. 2013. Urinary metabolite levels of pyrethroid insecticides in infants living in an agricultural area of the Province of Jiangsu in China. Chemosphere 90(11):2705–2713, PMID: 23270708, https://doi.org/10.1016/j.chemosphere.2012.11.050.
Xu C, Li X, Jin M, Sun X, Niu L, Lin C, et al. 2018. Early life exposure of zebrafish (Danio rerio) to synthetic pyrethroids and their metabolites: a comparison of

phenotypic and behavioral indicators and gene expression involved in the HPT axis and innate immune system. Environ Sci Pollut Res Int 25(13):12992–13003, PMID: 29480392, https://doi.org/10.1007/s11356-018-1542-0.

Xue Z, Li X, Su Q, Xu L, Zhang P, Kong Z, et al. 2013. Effect of synthetic pyrethroid pesticide exposure during pregnancy on the growth and development of infants. Asia Pac J Public Health 25(4 Suppl):72S–79S, PMID: 23966607, https://doi.org/10.1177/1010539513496267.

Yuen B, Boncompagni S, Feng W, Yang T, Lopez JR, Matthaei KI, et al. 2012. Mice expressing T4826I-RyR1 are viable but exhibit sex- and genotype-dependent susceptibility to malignant hyperthermia and muscle damage. FASEB J 26(3):1311–1322, PMID: 22131268, https://doi.org/10.1096/fj.11-197582.

Zheng J, Chen J, Zou X, Zhao F, Guo M, Wang H, et al. 2019. Saikosaponin D causes apoptotic death of cultured neocortical neurons by increasing membrane permeability and elevating intracellular Ca^{2+} concentration. Neurotoxicology 70:112–121, PMID: 30458186, https://doi.org/10.1016/j.neuro.2018.11.006.

Zimanyi I, Pessah IN. 1991. Pharmacological characterization of the specific binding of [^{3}H]ryanodine to rat brain microsomal membranes. Brain Res 561(2):181–191, PMID: 1666327, https://doi.org/10.1016/0006-8993(91)91594-Q.